Rho Kinase regulates neutrophil NET formation that is involved in UVB-induced skin inflammation

Minghui Li[1,2,3†], Xing Lyu[1,2,3†], James Liao[4], Victoria P. Werth[1,2]*, Ming-Lin Liu[1,2]*

[1] Corporal Michael J. Crescenz VAMC, Philadelphia, PA, 19104, USA

[2] Department of Dermatology, Perelman School of Medicine, University of Pennsylvania, Philadelphia, PA, 19104, USA

[3] Department of Rheumatology and Immunology, Tianjin Medical University General Hospital, Tianjin 300052, China

[4] Division of Cardiology, Department of Medicine, University of Chicago, Chicago, IL, USA

[†] Contribution equally

Running title: ***Li et al. Rho kinase and NETosis***

Key words: ***Rho kinase, Neutrophil, NETosis, UVB, Skin inflammation.***

Correspondence to Ming-Lin Liu, MBBS, PhD, Department of Dermatology, Perelman School of Medicine, University of Pennsylvania, and Philadelphia Veterans Administration Medical center, Philadelphia, PA 19104,
eMAIL: lium1@pennmedicine.upenn.edu,

Abstract

Objective. Ultraviolet B (UVB) is an important trigger of skin inflammation and lupus with leukocyte recruitment to inflamed skin. We recently reported the involvement of neutrophil NETosis in UVB-induced skin inflammation, and that NETotic nuclear envelope rupture is driven by PKCα-mediated nuclear lamin B disassembly. To address the role of Actin cytoskeleton in NETosis, we investigated the effects of Rho kinase (ROCK) and its downstream actomyosin cytoskeletal networks on PKCα nuclear translocation and NET formation, as well as their involvement in UVB-induced skin inflammation.

Methods. We studied the dynamic changes of ROCK and actomyosin cytoskeletal networks during NETosis induction and their involvement in PKCα nuclear translocation. Using mice with hematopoietic-specific ROCK1 deficiency, we investigated the effects of ROCK1 deficiency on NETosis, and its involvement in UVB-induced skin inflammation.

Results. We found that time course of nuclear translocation of cytosolic PKCα matched with the process of actin polymerization, and ROCK activation in the early stage of NETosis induction. Importantly, inhibition of actin polymerization or key molecules of the ROCK/MLCK/myosin pathway decreased nuclear translocation of PKCα and NET formation. Genetic deficiency of ROCK1, inhibited neutrophil NETosis *ex vivo* and *in vivo*, decreased the extracellular display of NET-associated IL-17A, TNFα, IFNγ, and IFNα in inflamed skin, and ameliorated skin inflammation in UVB-irradiated mice with hematopoietic-specific ROCK1 deficiency.

Conclusions. ROCK regulated NETosis in neutrophils through modulation of PKCα nuclear translocation via actomyosin cytoskeletal networks. ROCK1 deficiency ameliorated UVB-induced skin inflammation by attenuation of NETosis and extracellular display of NET-associated cytokines.

INTRODUCTION

Ultraviolet B (UVB) is an important trigger of cutaneous and systemic lupus erythematosus (CLE, SLE) [1-4]. UVB overexposure causes photodamage of skin with recruitment of inflammatory cells, including neutrophils [5]. A recent study has indicated that neutrophils are the critical early infiltrating immune cells within cutaneous lupus lesion in mice [6]. Several studies with transcriptional profiling analysis of lupus patient samples also confirmed the importance of neutrophils [7], and a gradual enrichment of neutrophil transcripts during lupus disease progression [8]. Therefore, it is important to understand the role of neutrophils in UVB-induced skin inflammation. NETosis is a unique form of neutrophil cell death with release neutrophil extracellular traps (NETs) [9, 10], which are involved in lupus pathogenesis [11, 12]. However, the involvement of NETosis in UVB-induced skin inflammation and the relevant cellular mechanisms are not well understood.

Nuclear chromatin forms the backbone of NETs, and thus nuclear envelope rupture is a required step for breaking the first physical barrier, nuclear chromatin release and extracellular NET formation [9, 10, 12]. We recently found that NETotic nuclear envelope rupture is driven by protein kinase C alpha (PKCα)-mediated phosphorylation and disassembly of nuclear lamin B [9] which is crucial to nuclear envelope integrity by forming highly organized meshworks surrounding the nuclear chromatin [13]. Furthermore, cyclin-dependent kinases (CDK)4/6 also control NETosis through regulation of lamin A/C phosphorylation [14]. Therefore, PKCα and CDK4/6 serve as NETotic lamin kinases [9, 10, 14] for regulation of nuclear lamina disassembly and NETotic nuclear envelope rupture.

PKCα exists diffusely in the cytosol of the unstimulated cells, and the kinase can be translocated to the nucleus during activation [15]. Schmalz et al indicated that nuclear translocation

of cytosolic PKCα requires intact cytoskeleton [16]. As an upstream regulator of cytoskeleton, Rho kinase (ROCK) inhibition blocks nuclear translocation and activation of PKC [17]. We have shown that PKCα nuclear translocation is required for nuclear lamina disassembly and NET formation [9]. Furthermore, functional cytoskeleton is required for NETosis induction [18-21] in the early stage, while actin cytoskeleton disassembly is also necessary for the plasma membrane rupture in the late stage of NETosis [10, 22].

It has long been known that Rho [23] and its effector kinase ROCK [24] regulate actin cytoskeleton organization. In the current study, we sought to investigate the dynamic changes of actin cytoskeleton and its upstream regulator ROCK, as well as its involvement in PKCα nuclear translocation during NETosis induction. Furthermore, F-actin and myosin motors form actin-myosin (actomyosin) cytoskeletal networks that are involved in nucleocytoplasmic shuttling [25]. The actomyosin cytoskeletal networks can be regulated by activation of myosin II and myosin regulatory light chain kinase (MLCK) through the ROCK/MLCK/myosin pathway [26]. Therefore, we also investigated the involvement of ROCK/MLCK/myosin pathway in PKCα nuclear translocation and NET formation *in vitro*. Importantly, we investigated the effects of ROCK1 deficiency on neutrophil NET formation *in vivo* and UVB-induced skin inflammation using mice with hematopoietic-specific ROCK1 deficiency.

METHODS

Mice

ROCK1 deficient mice ROCK1$^{+/-}$ on a C57BL/6J background were generated by Liao's laboratory as described before [27]. Since homozygous (ROCK1$^{-/-}$) mice always die perinatally,

heterozygous mice were used in this study. C57BL/6J wildtype (WT) and CD45.1 (B6.SJL-*Ptprc*^{a}*Pepc*^{b}/BoyJ) mice were purchased from Jackson Laboratory. All mice and their corresponding littermate controls were housed in a pathogen-free environment, and given food and water *ad libitum*. All animal experiments and animal protocols were approved by the Animal Care and Use Committee of University of Pennsylvania.

Generation of hematopoietic deficient mice by bone marrow transplantation (BMT)

To generate mice with hematopoietic-specific ROCK1 deficiency, or their corresponding background control mice, BMT was conducted according to our established BMT techniques by following the approved animal protocol, as described with modification [28]. In brief, the BM hematopoietic stem cells (HSCs, >5x10^{6} cells) were harvested from the femur and tibia of donor ROCK1$^{+/-}$ mice or their littermate WT (all 6-8-week-old, with CD45.2 congenic background). The donor HSCs (>5x10^{6} cells) from either ROCK1$^{+/-}$ or WT mice were transplanted into sex-matched CD45.1 recipient mice (all 6-8-week-old) which were pre-irradiated sub-lethally with two equal doses of 550 cGy (*Total Body Irradiation* 1100 cGy) at intervals of 18 hours [29, 30] with a *Cs-137 Irradiator* [28]. Starting one-week prior to BMT, mice were given medicated acidified water with antibiotics (sulfamethoxazole and trimethoprim) until 6 weeks post BMT. Mice were given soften food and kept in an animal biosafety level 2 room immediately after irradiation and BMT for up to 6 weeks until UVB exposure. Peripheral blood chimerism was analyzed by flow cytometry analysis of the reconstitution rate of CD45.2 cells in the peripheral blood of CD45.1 recipient mice at 4 weeks post BMT as a functional assay of HSC fitness. Only successfully transplanted mice (over 95% reconstitution) were used in later animal experiments.

UVB Exposure

The dorsal skins of CD45.1 mice with hematopoietic-specific ROCK1 deficiency (BMT-ROCK1$^{+/-}$) or their corresponding control mice (BMT-WT) were irradiated or not (sham groups) by UVB (150 mJ/cm^2/day) for 5 consecutive days under anesthetization by peritoneal injected Ketamine/Xylazine [9]. Each group included 6-8 mice with half males and half females. Animals were then sacrificed 24 hours after the last exposure. Whole dorsal skin samples, including epidermis, dermis, and subcutaneous fat were collected. Tissue sample sectioning was performed by the Penn Skin Biology and Diseases Resource-based Center. Skin sections from UVB-irradiated and sham mice were stained by hematoxylin and eosin (H&E). Infiltration of inflammatory cells was counted for the nucleated cells in the epidermis, dermis, or fat [31, 32].

Cell Culture and Treatment

Primary human neutrophils from the peripheral blood or mouse bone marrow (BM) neutrophils from the *femur* and *tibia* BM of WT vs ROCK1$^{+/-}$ [27] were isolated as described in our publication [9]. Mouse BM mPMNs were isolated with a neutrophil isolation kit (Miltenyl). Human HL-60 cell line were differentiated into polymorphic nuclear granulocytes (dPMNs) in RPMI-1640 with 10% FBS and 1.2% DMSO for 5-6 days as described in our published study [9]. Time course study of treatment of dPMNs by 50 nM PMA was conducted for 0 (for confocal microscopic imaging experiments, analysis started after 5 min of PMA stimulation to allow the suspension dPMNs to adhere in order to compare them with the adherent dPMNs at later time points), 15, 30, 60, 120, and 180 min, and then cells were fixed with 2% paraformaldehyde or lysed with cell lysis buffer for different experiments. All of the above primary human or mouse neutrophils or dPMNs were treated with, either PMA at 50-100 nM, or physiological NETosis-

inducer platelet-activating factor (PAF) [9] at 5-10 μM, for 1h or 3h without or with 30 min pretreatment with inhibitors of F-actin polymerization (Cytochalasin D), myosin II (Blebbistatin), myosin light chain (MLC) kinase (ML7), or ROCK (Y-27632, HA-1077, AS1892802), following by detection of NET formation or actin polymerization. For control conditions of confocal microscopic imaging experiments, 5 min of short stimulation by PMA to allow the suspension dPMNs to adhere in order to compare them with the adherent dPMNs at other conditions.

Detection of ROCK activity was performed with kit from Millipore. Briefly, neutrophil lysates from different time points were added to plate which were coated with recombinant Myosin phosphatase target subunit 1 (MYPT1) that contains a Thr696 residue ($MYPT1^{Thr696}$) which can be phosphorylated by ROCK1/2. Then a detection antibody that specifically detects $MYPT1^{Thr696}$ is applied, following by an HRP-conjugated secondary detection antibody, and chromogenic substrate. After adding stop solution, the absorbance signal detected at 450 nm reflects the relative amount of ROCK activity in the samples.

Assessment of NET Formation

All of the above primary human or mouse neutrophils or dPMNs were treated with either PMA (50 or 100 nM) or PAF (5 or 10 μM) for 3h. NET formation assessment and quantification was analyzed by either fluorometric NET quantification by SYTOX Green staining intensity, and/or immunofluorescent imaging quantification analysis by staining with impermeable DNA dye SYTOX Green for detection of NET formation, and the cell-permeable DNA dye SYTO Red to count the total number of neutrophils, as described before [9].

Flow cytometry analysis

For detection of polymerized filamentous actin (F-actin), the 2% paraformaldehyde (PFA) fixed neutrophils from different time points (time course) after PMA stimulation, or PMA-stimulated dPMN cells or mouse primary BM neutrophils without or with pretreatment by ROCK inhibitors were stained by phalloidin-RFP or phalloidin-FITC and analyzed with flow cytometry according to published methods [33]. To detect the indirect effects of UVB through PAF [34] and direct effects of UVB irradiation on cytokine induction, the BM neutrophils from ROCK1$^{+/-}$ vs WT were treated for overnight without or with PAF, without or with isolated NETs (for IFNα induction). Then the treated cells were fixed with 2% PFA and permeabilized with 0.1% Triton X-100, and stained by FITC- or Alexa488-conjugated primary antibodies against IL-17A, TNFα, IFNγ, or IFNα (Biolegend or Bioss). The analysis of actin polymerization (detected by RFP- or FITC-conjugated phalloidin), and expression of cytokines or CXCR2 in BM neutrophils were based on gated cells that were positive in neutrophil marker ly6G (PE-labeled). Furthermore, to detect the reconstitution rate of donor-derived cells in the peripheral blood of BMT mice, blood samples were harvested from the saphenous vein of all mice 4 weeks after the BMT procedure. Erythrocytes were then removed by hypotonic lysis (0.2% $NaCl_2$), and stained with PE-labeled anti-mouse CD45.1 and FITC-labeled anti-mouse CD45.2, following by flow cytometry analysis as described before [35].

Transmigration Assays

The pore transmigration ability of primary neutrophils from WT vs ROCK1$^{+/-}$ mice was examined as described before [9] by using Boyden chamber, 24-well trans-well plates with 3 μm pore inserts, under stimulation with CXCL-1 (100 ng/ml). The pore transmigration ability was

expressed as relative transmigration compared to that in control neutrophils of the mice without treatment.

Fluorescent Immunocytochemistry and Immunohistochemistry analysis

For immuno-cytochemistry analysis, dPMNs or mouse BM neutrophils were treated without or with different inhibitors, then treated without or with PMA or PAF for 1-3h for study of PKCα nuclear translocation. Then the treated cells were stained by primary anti-total PKCα or anti-lamin B Abs, followed by secondary Abs with FITC or PE conjugation [9]. For the *ex vivo* NETosis induction with exhibition of NET-associated cytokines, the BM neutrophils from ROCK1$^{+/-}$ vs WT were treated for 20h without or with PAF, without or with isolated NETs (for IFNα induction). Then the treated cells were fixed with 2% PFA and permeabilized with 0.1% Triton X-100, and stained by primary antibodies against IL-17A, TNFα, IFNγ, or IFNα with FITC- or Alexa488-conjugation (Biolegend or Bioss). The neutrophil marker Alexa-647-labeled anti-ly6G was used. DNA was stained with DAPI.

The paraffin-embedded skin tissue sections were stained as described before [9]. The neutrophil markers Alexa-647-labeled anti-ly6G were used for detection of neutrophils and NETosis in combination with DNA staining with DAPI as described [9]. FITC- or Alexa488-conjugated primary antibodies against IL-17A, TNFα, IFNγ, or IFNα were used to stain cytokines (Biolegend or Bioss). Slides were mounted with Gold Antifade Mountant (Invitrogen). Confocal fluorescent images were analyzed with an Olympus Fluoview 1000 confocal microscope.

Statistical analyses

GraphPad Prism 6 was used to perform statistical analysis. Data are shown as means ± standard deviations (SD). Normality distribution of the sample sets was first analyzed. Comparisons amongst three or more groups were performed using ANOVA followed by Student-Newman-Keuls analysis for sample sets with normal distribution, or using Kruskall-Wallis analysis followed by Dunn´s test for same sets with a non-normal distribution. Comparisons between two groups were conducted with student's t-test. Pearson correlation analysis was used when applicable. Statistical significance was considered at a level of P-value < 0.05.

RESULTS

Disruption of actin cytoskeleton or actomyosin cytoskeletal networks attenuated neutrophil NET formation

Nuclear envelope rupture is regulated by PKCα-mediated lamin B disassembly [9, 10], and nuclear translocation of PKCα requires intact cytoskeleton [16, 21, 36]. In addition, actomyosin networks have been shown to be important in nucleocytoplasmic shuttling [25]. In the current study, we found that disruption of actin cytoskeleton filaments by inhibition of actin polymerization with cytochalasin D, or disruption of actomyosin cytoskeletal networks by inhibition of myosin II or its upstream MLCK with Blebbistatin or ML7 correspondingly, significantly decreased PMA- or PAF-induced NETosis in human or mouse neutrophils (Figure 1A-C). Importantly, disruption of actin cytoskeleton by cytochalasin D or inhibition of myosin II or MLCK by Blebbistatin or ML7 increased cytosolic retention of PKCα and attenuated nuclear translocation of PKCα, observed at 60 min after PMA stimulation (Fig 1D-F). Interestingly, the nuclei of these cells still remained as multiple lobes similar as those in control cells (Fig 1D-F). In

contrast, we saw the swelling nuclei with disintegrated nuclear envelope in cells treated with PMA alone (Fig 1D). These results suggested that not only actin cytoskeleton, but also the actomyosin cytoskeletal networks, are important for nuclear translocation of PKCα and nuclear envelope rupture (Fig 1G), which is required for nuclear chromatin extrusion and NET formation [9, 10]. Along this line, other studies also reported the involvement of actin cytoskeleton [37] or myosin II [38] in nuclear translocation of cytosolic molecules, and in actomyosin-dependent nucleocytoplasmic shuttling [25].

ROCK regulated PKCα nuclear translocation by modulation of actin cytoskeleton polymerization in neutrophils

To understand the potential role of actin cytoskeleton and its upstream regulator ROCK in PKCα nuclear translocation, we investigated the time course of PKCα nuclear translocation, the dynamic changes of actin polymerization, and Rho kinase activation in PMA-stimulated cells from 0 to 3h. As we have shown in our recent publication [9], the diffusely distributed cytosolic PKCα in PMA-stimulated cells gradually translocated to the nucleus within 60 minutes of PMA stimulation (Fig 2A-C), as compared to those at initial time point (analysis started after 5 min PMA stimulation to allow the suspension neutrophils to adhere in order to compare with the adherent neutrophils at later time points for microscopic analysis). Alone with the nuclear accumulation of lamin kinase PKCα, PKCα-mediated nuclear lamin B disassembly resulted in nuclear envelope disintegration at 60 min (Fig 2A), followed by nuclear DNA extracellular extrusion from small rupture sites at 120 min (Fig 2A), and the extracellular release of large amounts of nuclear DNA from the enlarged rupture of the nuclear envelope at 180 min (Fig 2A) after PMA stimulation,

resulting in extracellular NET formation with the collapse of the nuclear and plasma membranes [9, 10].

Since previous [18-21] and the current (Fig 1A-G) works have shown that functional cytoskeleton is required for NETosis induction in the early stage of the process, and PKCα nuclear translocation requires intact cytoskeleton [16], we thought to look the dynamic changes of actin polymerization. Previous works reported that there is basal F-actin polymerization in unstimulated resting cells [39, 40] and actin reorganization could be started in "second" after cell stimulation [40, 41]. In the current study, we also found basal F-actin assembly in the unstimulated resting neutrophils (Fig 2D). Following PMA stimulation, we found time-dependently increased percentage of cells with actin polymerization and F-actin filament formation at 15 and 30 min, reached a peak by 60 min time point, following by gradual actin depolymerization at 120 and 180 min (Fig 2D,E). In line with these observation, previous studies reported that PMA can induce actin polymerization in neutrophils and lymphocytes [36, 42]. Our results suggest that PMA-induced actin polymerization provides structural basis for nuclear translocation of PKCα [16] for at least 60 min (Fig 2D,E), while actin cytoskeleton disassembly at 120 and 180 min (Fig 2D,E) which may be responsible for the plasma membrane rupture and nuclear DNA extracellular release in the corresponding time points (Fig 2A), similar to the phenomenon reported by Thiam and coauthors [22], as cortical cytoskeletal networks are important for plasma membrane integrity [10].

Interestingly, PMA stimulation increased ROCK activity at 15 and 30 min, and peaked at 60 min time point (Fig 2F), which are tightly matched with the dynamic changes of F-actin polymerization within 60 min of PMA stimulation (Fig 2D,E). Then, ROCK activity was gradually reduced, with significant decrease at 180 min as compared to that at 60 min (Fig 2F), corresponding to the gradual disassembly of actin cytoskeleton at 2-3h time points (Fig 2D,E). Therefore, the

dynamic changes of actin polymerization/depolymerization (Fig 2D,E) with its matched corresponding changes of up/down in ROCK activity (Fig 2F) may help to explain nuclear translocation of PKCα by functional cytoskeleton in the early stage, and plasma membrane rupture with the actin depolymerization [22] in the late stage of NETosis. Therefore, actin cytoskeleton and its upstream molecule ROCK play an important role in NETosis.

Since Rho and its effector kinase ROCK regulate actin cytoskeleton organization in previous studies [23, 24], here we tested the role of ROCK in actin polymerization in neutrophils during NETosis. We found that inhibition of ROCK activation by ROCK inhibitor Y27632 resulted in impaired actin polymerization not only in primary mouse BM neutrophils (Fig 2G,H), but also in human dPMNs (Suppl Fig 1C). Additionally, genetic deficiency of ROCK1 attenuated actin polymerization in neutrophils from ROCK1 deficient mice as compared to those from WT mice (Fig 2I,J). Similarly, Gallo et al reported that ROCK1 inhibition impaired actin polymerization in cells transfected by silencing shRNA [43]. Therefore, the above results by pharmacological or shRNA silencing inhibition, or genetic deficiency, of ROCK from our and other studies [43] suggest the role of ROCK in actin polymerization. Furthermore, inhibition of ROCK by different inhibitors increased cytosolic retention of PKCα, and attenuated PKCα nuclear translocation in neutrophils (Fig 2K, Suppl Fig 1A,B), decreasing nuclear envelope disintegration (Fig 2K). Therefore, our and other studies support the role of actin cytoskeleton [16] and its upstream ROCK/MLCK/ myosin pathway (Fig 1D-F, 2K, Suppl Fig 1A,B) in nuclear translocation PKCα that is crucial to nuclear envelope rupture and extracellular release of nuclear DNA during NETosis [9, 10].

Taken together, our results demonstrated that PMA-induced reorganization of actin cytoskeleton and its upstream upstream ROCK/MLCK/ myosin pathway (Fig 1-2) are involved in

nuclear translocation of lamin kinase PKCα [16], which drives nuclear envelope rupture for nuclear DNA extrusion [9, 10]. Furthermore, the reduced ROCK activity and actin depolymerization in the late stage (Fig 2D-F) may be responsible for plasma membrane rupture [22] for DNA extracellular release and NET formation [10]. In line with our study, several previous works also reported the involvement of actin cytoskeleton in NETosis [18-21]. The current work provides more detailed investigation and mechanistic explanation in this context.

Inhibition of ROCK by pharmacological inhibition or genetic ROCK1 deficiency attenuated NET formation in neutrophils *in vitro* or *ex vivo*

To explore the role of ROCK in NETosis, we found that inhibition of ROCK with different chemical inhibitors (Y27632, HA1077, AS1892802) significantly decreased NET formation *in vitro* in dPMNs (Fig 3A) and primary human neutrophils (Fig 3B) stimulated by PMA, or in mouse neutrophils stimulated by PAF (Fig 3C), detected by different approaches. Most importantly, genetic deficiency of ROCK1 inhibited NETosis *ex vivo* in BM neutrophils from ROCK1$^{+/-}$ mice as compared to those from their WT littermates (Fig 3D,E). Taken together, ROCK activation (Fig 2F) regulated actin polymerization (Fig 2D,E) which mediated nuclear translocation of PKCα that drives nuclear envelope rupture (Fig 2A) for nuclear DNA extrusion. Importantly, inhibition of ROCK impaired actin polymerization (Fig 2G-J), decreased PKCα nuclear accumulation (Fig 2K), and attenuated NETosis in neutrophils *in vitro* or *ex vivo* (Fig 3A-E). Therefore, these results from *in vitro* and *ex vivo* experiments indicate that ROCK signal pathway regulated NETosis by modulation of nuclear translocation of PKCα and nuclear envelope rupture through regulation of actomyosin cytoskeletal networks (Suppl Fig 1D).

Hematopoietic-specific ROCK1 deficiency protected mice from UVB-induced skin inflammation

To study the effects of ROCK1 on neutrophil NETosis *in vivo* and its involvement in UVB-induced skin inflammation, we generated mice with hematopoietic-specific ROCK1 deficiency by transplantation of BM HSCs from ROCK1$^{+/-}$ mice or their WT littermates to CD45.1 recipient mice, following by irradiation of these mice without or with UVB (Suppl Fig 2A). Four-weeks after the BMT procedure, the reconstitution status of donor-derived cells (CD45.2) in peripheral blood of recipient CD45.1 mice was examined by flow cytometry for each BMT mouse. Only the recipient mice with over 95% reconstitution rates (Suppl Fig 2B) were included for the following studies. To further confirm high reconstitution in mice with successful BMT, we found that majority of infiltrated neutrophils were donor-derived CD45.2 neutrophils (Suppl Fig 2C), but not the host CD45.1 neutrophils (Suppl Fig 2D), in skin lesions of UVB-irradiated CD45.1 recipient mice who received BMT of HSCs from WT donors.

With these mice, we found decreased dermal skin thickness, and reduced inflammatory cell infiltration in dermal skin of UVB-irradiated BMT-ROCK1$^{+/-}$ mice as compared to those in BMT-WT control mice (Fig 4A,C,D), however, the differences of epidermal skin thickness in BMT-ROCK1$^{+/-}$ vs BMT-WT mice were not significant (Fig 4B). Interestingly, inflammatory cell infiltration in skin was positively correlated with dermal skin thickness in all experimental mice (Fig 4E). Furthermore, fluorescent staining of skin sections of these mice demonstrated decreased NET formation *in vivo* in skin lesions of UVB-irradiated BMT-ROCK1$^{+/-}$ mice as compared to those of BMT-WT control mice (Fig 4F,G). Importantly, distribution area of neutrophil NETs in inflamed skin was positively correlated with dermal skin thickness (Fig 4H), indicating the involvement of neutrophil NETs in skin inflammation.

To understand the role of ROCK1 deficiency in skin inflammation with neutrophil NETosis, we found the mildly decreased chemotactic migration ability *in vitro* in ROCK1 deficient neutrophils as compared to that in WT neutrophils (Fig 4I). In line, a previous study by our co-author reported that ROCK1 deletion reduced CXCL1/CXCR2-mediated migration capability in macrophages derived from bone marrow of ROCK1 deficient mice [44]. Furthermore, no differences in CXCR2 expression in BM neutrophils from WT vs ROCK1$^{+/-}$ mice were observed (Suppl Fig 2E,F). Generally, cell migration is affected by cellular factors (including cytoskeleton) and environmental factors (including chemotactic signals) [45]. Therefore, the above results indicated the effect of destabilized actin cytoskeleton on impaired chemotactic migration ability in ROCK1 deficient neutrophils. These results may explain in part the reduced infiltration of inflammatory cells (Fig 4D), particularly neutrophils (Fig 4J), in inflamed skin of UVB-irradiated BMT-ROCK1$^{+/-}$ mice as compared to those in BMT-WT controls. However, the mildly reduced chemotactic migration ability of heterogeneous ROCK1 deficient neutrophils in vitro seems insufficient to explain the ameliorated skin inflammation in UVB-irradiated BMT-ROCK1$^{+/-}$ mice as compared to those in their BMT-WT controls (Fig 4A-D,J).

Recent studies demonstrated that NETs have chemotactic function to promote cancer cell metastasis [46] or enhance monocyte infiltration by induction of MCP1 expression in endothelial cells [47]. Here, we found decreased NETosis *in vitro* in human or mouse neutrophils with ROCK inhibitors (Fig 3A-C), and *ex vivo* in neutrophils from ROCK1$^{+/-}$ mice (Fig 3D,E). Most importantly, we found a significantly reduced percentage of NET formation *in vivo* among neutrophils infiltrated to the inflamed skin of UVB-irradiated BMT-ROCK1$^{+/-}$ mice as compared to those in BMT-WT mice (Fig 4K). Therefore, the attenuated skin inflammation in UVB-irradiated BMT-ROCK1$^{+/-}$ mice may, at least in part, be attributed to the reduced NET formation

by ROCK1 deficiency (Fig 4A,F,G). Our published work has shown that neutrophil NETs can display IL-17A and TNFα, the cytokines with chemotactic properties, in skin of UVB-irradiated mice [9]. Next, we sought to look the effects of ROCK1 deficiency on display of NET-associated cytokines in skin of UVB-irradiated BMT-ROCK1$^{+/-}$ mice.

Hematopoietic-specific ROCK1 deficiency decreased the exhibition of pro-inflammatory cytokines by neutrophil NETs in BMT-ROCK1$^{+/-}$ mice

We found that UVB exposure increased formation of NETs with exhibition of NET-associated IL-17A, TNFα, IFNγ, or IFNα in inflamed skin of BMT-WT mice (Fig 5A-I). Importantly, hematopoietic-specific ROCK1 deficiency can attenuate neutrophil NETosis *in vivo* and its display of NET-associated cytokines in UVB-irradiated skin of BMT-ROCK1$^{+/-}$ mice (Fig 5A-I). Many cytokines have chemotactic properties for recruitment of inflammatory cells [48-50]. Here, we found NET-associated IL-17A or TNFα in inflamed skin in UVB-irradiated BMT-WT mice (Fig 5A-I) similar to what we found in UVB-irradiated mice in our recent publication [9]. Previous works have reported that IL-17A [48], together with TNFα [49], can synergistically induce leukocyte infiltration to sites of inflammation [51]. Furthermore, NET-associated IFNγ together with IL-17A also promote leukocyte recruitment in another study [50]. Thus, extracellular display of NET-associated IL-17A, TNFα, and IFNγ in skin contributes to further recruitment of leukocytes and their accumulation in certain areas of skin dermis, as well as propagation of inflammatory responses in inflamed skin of UVB-irradiated BMT-WT mice (Fig 4F, 5C). Importantly, there were fewer and diffusely distributed non-netting leukocytes in skin of UVB-irradiated BMT-ROCK1$^{+/-}$ mice (Fig 4F, 5C). Under UVB irradiation, the neutrophil NETs and their associated cytokines with relatively high concentrations in the local skin likely contributed

to further recruitment of leukocytes to skin of BMT-WT mice. In contrast, the non-netting neutrophils may secrete their cytokines to extracellular space that always quickly diffused to blood stream and are diluted by the circulation of UVB-irradiated BMT-ROCK1$^{+/-}$ mice. Therefore, the above feature may partly explain the fewer leukocyte infiltration in skin of UVB-irradiated BMT-ROCK1$^{+/-}$ mice (Fig 4F, 5C). In addition to above cytokines, we also detected NET-associated IFNα, an important cytokine that is crucial to pathogenesis of SLE [52, 53] and important to UVB-induced skin inflammation [32]. More importantly, NET-associated IL-17A, TNFα, IFNγ, and IFNα in skin were positively correlated with dermal skin thickness in all experimental mice (Suppl Fig 3).

ROCK1 genetic deficiency inhibited formation of NETs *ex vivo* and their display of pro-inflammatory cytokines in neutrophils from ROCK1 deficient mice

Previous publications have reported that neutrophils can express and produce various cytokines, including IL-17A [50], TNFα [54], IFNγ [55], or IFNα [56]. Studies from our and other groups have reported that neutrophil-expressed cytokines can be released with NETs [9, 56]. Recently, Agak et al demonstrated that extracellular traps released by TH17 cells can also be associated with their expressed IL-17 [57]. In the current study, we found the display of NET-associated cytokines in UVB-irradiated skin (Fig 5). To determine if these NET-associated cytokines were derived from their parental neutrophils, we conducted *ex vivo* experiments by treatment of mouse neutrophils with PAF, a physiologic NETosis inducer that can be released from keratinocytes after UVB irradiation [9, 58]. We found that PAF stimulation can induce expression of IL-17A, TNFα, IFNγ, and IFNα (with PAF+NETs) in mouse BM neutrophils, detected by flow cytometry analyses (Fig 6A,D,G,J, suppl Fig 4). Interestingly, these PAF-induced IL-17A, TNFα,

IFNγ, and IFNα in mouse neutrophils can be released from their parental neutrophils to the extracellular space during NET formation (Fig 6B,C,E,F,H,I,K,L).

ROCK1 deficiency attenuated PAF-induced TNFα (Fig 6D, suppl Fig 4B), but did not affect expression of IL-17A, IFNγ, and IFNα (Fig 6A,G,J, suppl Fig 4) in BM neutrophils from ROCK1$^{+/-}$ mice as compared to those from WT mice. Importantly, ROCK1 deficiency attenuated NET formation with decreased area of extracellular display of NET-associated cytokines by enclosing them within non-netting neutrophils from ROCK1$^{+/-}$ mice as compared to those from WT mice (Fig 6B,C,E,F,H,I,K,L). Under UVB irradiation, PAF from keratinocytes can trigger neutrophils to form NETs that exhibit proinflammatory cytokines, which further recruited leukocytes, therefore resulting in increased inflammatory cell accumulation in skin, particularly in the epidermal-dermal junction area of inflamed skin (Fig 4F,5C). Although ROCK1 deficiency did not affect some cytokines for their cellular expression (Fig 6A,D,G,J, suppl Fig 4), inhibition of NET formation by ROCK1 deficiency however decreased their extracellular display with NETs by increasing their intracellular retention, thus resulting in reduced leukocyte recruitment in skin with ameliorated skin inflammation in UVB-irradiated BMT-ROCK1$^{+/-}$ mice.

DISCUSSION

Photosensitive skin reaction is a complex inflammatory response to UVB-induced skin tissue damage [2, 4, 59, 60]. UVB overexposure causes epidermal keratinocyte apoptosis and DNA damage [60, 61], and accumulation of dead cell extracellular DNA may initiate autoimmune responses for lupus development [4]. In addition, other types of cell death have also been shown to contribute to extracellular DNA accumulation, and lupus pathogenesis [62]. Histopathologic

analysis of skin lupus indicates the potential interaction of between immune cells and epidermal keratinocytes [60, 63]. UVB irradiation of keratinocytes releases PAF, which contributes to the sustained inflammatory responses [34], inducing neutrophil recruitment and NETosis in inflamed skin [9]. Studies from our and other groups [9, 58] have shown that PAF can serve as a natural stimulus for induction of NETosis. On the other hand, direct exposure of neutrophils to UV can also induce NET formation *in vitro* [9, 64]. Therefore, NET formation *in vivo* in UVB-irradiated skin may be attributed to indirect effects of UVB through PAF [34] and direct effects of UVB irradiation [9, 64] on neutrophils infiltrated to the inflamed skin.

Over the past decade, various signaling pathways have been reported to be involved in NETosis, i.e., NADPH oxidase (NOX)-dependent vs -independent, reactive oxygen species (ROS)-dependent vs -independent etc [65-67]. Given that nuclear chromatin forms the backbone of NETs, the nucleus is the root of nuclear DNA extracellular traps [10, 68-72]. Thus, decondensation of nuclear chromatin is required for its externalization, while rupture of the nuclear envelope and plasma membrane are the necessary steps for removal of the physical barriers of nuclear membranes for nuclear DNA discharge and extracellular NET formation [10]. Therefore, these key cellular morphological changes in nuclear chromatin, nuclear envelope, and plasma membrane are required for extracellular DNA NET formation [9, 10, 14, 71, 72] no matter if NETosis is NOX- or ROS-dependent or –independent.

We recently reported that NETotic nuclear envelope rupture is driven by PKCα-mediated nuclear lamin B disassembly [9]. In the current study, we found that nuclear translocation of cytosolic PKCα [9, 15] was regulated by actin cytoskeleton [16], actomyosin cytoskeletal networks and their upstream ROCK in the early stage of NETosis induction. In line, Hippenstiel demonstrated that inhibition of ROCK blocks nuclear translocation and activation of PKC in

endothelial cells [17], and Matoba reported the role of ROCK in nuclear translocation of other cytosolic molecules through regulation of actin cytoskeleton organization [73]. Other studies also report the involvement of actin cytoskeleton filament [37], or myosin II [38], or actomyosin-dependent [25] in nucleocytoplasmic shuttling. Therefore, the current study provides a cellular mechanistic explanation for the role of actin cytoskeleton in early stage of NETosis induction [18, 21], in which nuclear translocation of NETotic lamin kinase PKCα is mediated by actin cytoskeleton [16], and its upstream ROCK signaling pathway [17] during NETosis. In addition to their role in nuclear-cytoplasmic shuttling [25], ROCK and its-regulated actomyosin cytoskeletal networks may also enable nuclear deformation and contribute to nuclear envelope rupture by forces generated by the cytoskeletal networks [74]. However, it is still unclear if actomyosin cytoskeletal networks also contribute to NETotic nuclear envelope rupture by tearing the disassembled nuclear lamina with their "forces".

Plasma membrane is the final physical barrier for extracellular release of nuclear chromatin and NET formation. The cell cortex is a layer of cytoskeletal networks underneath the plasma membrane, consisting of F-actin filaments, myosin motors, and actin-binding proteins [75]. The contractile forces generated by cortical cytoskeletal networks are important for maintenance of plasma membrane integrity [75]. In contrast to ROCK activation and actin cytoskeleton polymerization in the early stage of NETosis induction, their dynamic changes after the peak time point (60 min) turned to gradually decrease in ROCK activity with actin cytoskeleton disassembly during the late stage of NETosis induction. The late stage actin cytoskeleton disassembly may contribute to the plasma membrane rupture for NET release as reported in a recent study [22].

UVB-induced skin inflammation manifested as increased skin thickness, enhanced inflammatory cell infiltration, and elevated proinflammatory cytokine expression. ROCK and its

regulated actin cytoskeletal networks serve as cellular factors to modulate cell migration [45]. Wang and colleagues demonstrated that macrophages with ROCK1 deletion from ROCK1$^{-/-}$ mice showed significantly impaired chemotactic migration ability [44]. In the current study, we found the mildly decreased transmigration *ex vivo* in transwell migration experiments in neutrophils with heterogeneous ROCK1 deficiency, and the significantly reduced leukocyte infiltration *in vivo* with diffusely distributed non-netting neutrophils in skin of UVB-irradiated BMT-ROCK1$^{+/-}$ mice. These results suggest that the reduced ROCK1 expression in leukocytes of ROCK1$^{+/-}$ mice [27] can still partly regulate actomyosin cytoskeletal networks that drive cell movement. In the meantime, the reduced ROCK1 expression can inhibit NETosis in neutrophils through interfering with cytosolic PKCα nuclear translocation that induces nuclear envelope rupture [9].

We have recently demonstrated the involvement of NETs and NET-associated cytokines in UVB-induced skin inflammation [9], and others also demonstrated association of IL-17 with neutrophil NETs [76] or extracellular traps released by TH17 cells [57]. In the current study, we found PAF-induced expression of IL-17A, TNFα, IFNγ, and IFNα in neutrophils, and these cytokines can be released to the extracellular space with NETs during NETosis. Furthermore, ROCK1 deficiency not only inhibited TNFα expression in neutrophils, but also attenuated NETosis and TNFα release with NETs ex vivo, thus contributing to the decreased skin inflammation in UVB-irradiated BMT-ROCK1$^{+/-}$ mice. Several other studies have shown that inhibition of ROCK can attenuate TNFα expression in different cells in various scenario [77, 78]. However, we did not see significant effects of ROCK1 deficiency on neutrophil expression of IL-17A, IFNγ and IFNα cytokines in the current study. Several papers have reported that ROCK2 isoform, but not ROCK1, regulates IL-17 and IFN-γ secretion from T cells [79, 80], as IL-17 production can be inhibited by either ROCK2 genetic deficiency [79], or ROCK2 siRNA silencing

or ROCK2 specific inhibitor KD025 [80]. In addition, KD025 can attenuate IFN-γ production, while ROCK1 siRNA silencing does not affect IFN-γ production [80]. These studies helped us to understand our results of unchanged IL-17A and IFNγ in ROCK1 deficient neutrophils as compared to the WT cells. However, there is no published work regarding the effects of ROCK in IFNα expression. Although no changes were observed in neutrophil expression of several cytokines, ROCK1 deficiency can inhibit NET formation and decrease extracellular display of NET-associated IL-17A, IFNγ and IFNα ex vivo, and in vivo in skin of UVB-irradiated BMT-ROCK1$^{+/-}$ mice. Taken together, decreased extracellular exhibition of NET-associated IL-17A, TNFα, IFNγ, and IFNα may be responsible for the attenuated leukocyte recruitment and skin inflammation in UVB-irradiated BMT-ROCK1$^{+/-}$ mice.

Using mice with genetic deficiency, Li et al reported that both IL-17A and IFN-γ can be produced by neutrophils and can positively regulate neutrophil infiltration [50]. Importantly, we recently demonstrated that blockage of TNFα with anti-TNFα significantly inhibited UVB-induced recruitment of inflammatory cells [81]. In contrast to the freely secreted cytokines that can be diffused to circulation with large dilution by circulating blood, the NET-associated cytokines may be retained in the local skin at a relatively high concentration for longer period of time, thus sustaining and propagating inflammatory responses in UVB-irradiated skin. All of the above support the role of NET-associated IL-17A, TNFα, or IFNγ cytokines in inflammatory cell recruitment to skin of UVB irradiated mice, while inhibition of NET formation with decreased extracellular display of NET-associated cytokines may at least partly explain the attenuated infiltration of leukocytes in inflamed skin of BMT-ROCK1$^{+/-}$ mice. In line with the current study, recent publications demonstrated that NETs can act as a chemotactic factor with NET-associated

components, i.e. human LL-37 [82] or mouse CRAMP [83], to promote cell migration, including cancer cell metastasis [46]. On the other hand, NETs may enhance monocyte infiltration by induction of MCP1 expression in endothelial cells [47].

In addition to the above discussed chemotactic effects of NET-associated cytokines, NET-associated IFNγ and IFNα not only contribute to UVB-induced skin inflammation [60, 84], but are also involved in lupus pathogenesis [85-87]. Although plasmacytoid dendritic cells are professional cells for IFNα production, recent works indicate that neutrophils may also express IFNα in the presence of chromatin [56]. In the current study, we found NETotic neutrophils express IFNα *in vivo* in skin of UVB-irradiated BMT-WT mice, probably triggered by DNA released from NETotic neutrophils nearby in inflamed skin, while ROCK1 deficiency may decrease IFNα expression through inhibition of DNA NET exposure in skin of BMT-ROCK1$^{+/-}$ mice. This is also confirmed by our *ex vivo* experiments in which IFNα expression in neutrophils can be produced by co-stimulation with PAF and isolated NETs. Since IFNα is a major driver of lupus pathogenesis, our results suggest that NETs and their associated IFNα may contribute to photosensitivity in lupus. Isgro et al reported enhanced ROCK activation in SLE patients with increased Th17 cell differentiation, and inhibition of ROCK attenuated IL-17 production in SLE patients [88]. Thus, ROCK might be a potential target for regulation of T cell dysfunction in SLE [89]. Interestingly, the current study demonstrated that ROCK might be a potential target for treatment of UVB-induced skin inflammation due to its role in regulation of NET formation.

Taken together, ROCK regulated NET formation in neutrophils by modulation of nuclear translocation of PKCα through actomyosin cytoskeletal networks. ROCK1 deficiency ameliorates UVB-induced skin inflammation by attenuation of NET formation and its display of NET-associated cytokines. The current study demonstrates the contribution of NETosis to UVB-induced

skin inflammation and photosensitivity in lupus, thus providing insights into novel therapeutics in NETosis-related human diseases, including lupus.

AUTHOR CONTRIBUTIONS

Liu conceived and designed the study. Li, Lyu, Liu performed the laboratory experiments and acquired the experimental data. For the microscopic image analysis, Liu, Lyu, Li took the images, Lyu and Li conducted further quantification and statistical analysis. Liu, Lyu, and Werth analyzed and interpreted the data and finalized the paper. Li, Lyu, Liao, Werth and Liu were involved in preparation and revision of the manuscript. All authors read and approved the final manuscript.

ACKNOWLEDGEMENTS

The authors would like to acknowledge Penn Skin Biology and Diseases Resource-based Center for their skin histology service. The authors would thank Debra A. Pawlowski (animal facility, Philadelphia VA Medical Center) for her kindly help with our animal experiments. This work was supported by Lupus Research Alliance (416805) and NIH R21AI144838 (to MLL), the Veterans Affairs Merit Review Award (to VPW), and NIH HL052233 and HL136962 (to JL).

CONFLICT OF INTEREST

The authors have no conflict of interests to declare.

References

1. Werth, V.P. et al. (2004) Photosensitivity in rheumatic diseases. J Investig Dermatol Symp Proc 9 (1), 57-63.
2. Doerner, J. et al. (2016) Fn14 deficiency protects lupus-prone mice from histological lupus erythematosus-like skin inflammation induced by ultraviolet light. Exp Dermatol 25 (12), 969-976.
3. Deng, G.M. and Tsokos, G.C. (2015) Pathogenesis and targeted treatment of skin injury in SLE. Nat Rev Rheumatol 11 (11), 663-9.
4. Wenzel, J. (2019) Cutaneous lupus erythematosus: new insights into pathogenesis and therapeutic strategies. Nat Rev Rheumatol 15 (9), 519-532.
5. Rodero, M.P. et al. (2014) Differential effects of ultraviolet irradiation in neonatal versus adult mice are not explained by defective macrophage or neutrophil infiltration. J Invest Dermatol 134 (7), 1991-7.
6. Han, X. et al. (2019) PD-1H (VISTA)-mediated suppression of autoimmunity in systemic and cutaneous lupus erythematosus. Sci Transl Med 11 (522).
7. Panousis, N.I. et al. (2019) Combined genetic and transcriptome analysis of patients with SLE: distinct, targetable signatures for susceptibility and severity. Ann Rheum Dis 78 (8), 1079-1089.
8. Banchereau, R. et al. (2016) Personalized Immunomonitoring Uncovers Molecular Networks that Stratify Lupus Patients. Cell 165 (3), 551-65.
9. Li, Y. et al. (2020) Nuclear envelope rupture and NET formation is driven by PKCα-mediated lamin B disassembly. EMBO Rep 21 (e48779).

10. Liu, M.L. et al. (2021) Recent progress in the mechanistic understanding of NET formation in neutrophils. FEBS J.
11. Kahlenberg, J.M. et al. (2013) Neutrophil extracellular trap-associated protein activation of the NLRP3 inflammasome is enhanced in lupus macrophages. J Immunol 190 (3), 1217-26.
12. Lood, C. et al. (2016) Neutrophil extracellular traps enriched in oxidized mitochondrial DNA are interferogenic and contribute to lupus-like disease. Nat Med 22 (2), 146-53.
13. Goldberg, M.W. et al. (2008) Filaments made from A- and B-type lamins differ in structure and organization. J Cell Sci 121 (Pt 2), 215-25.
14. Amulic, B. et al. (2017) Cell-Cycle Proteins Control Production of Neutrophil Extracellular Traps. Dev Cell 43 (4), 449-462.
15. Zauli, G. et al. (1996) Nuclear translocation of protein kinase C-alpha and -zeta isoforms in HL-60 cells induced to differentiate along the granulocytic lineage by all-trans retinoic acid. Br J Haematol 93 (3), 542-50.
16. Schmalz, D. et al. (1996) Transport of protein kinase C alpha into the nucleus requires intact cytoskeleton while the transport of a protein containing a canonical nuclear localization signal does not. J Cell Sci 109 (Pt 9), 2401-6.
17. Hippenstiel, S. et al. (1998) Rho protein inhibition blocks protein kinase C translocation and activation. Biochem Biophys Res Commun 245 (3), 830-4.
18. Neeli, I. et al. (2009) Regulation of extracellular chromatin release from neutrophils. J Innate Immun 1 (3), 194-201.
19. Stojkov, D. et al. (2017) ROS and glutathionylation balance cytoskeletal dynamics in neutrophil extracellular trap formation. J Cell Biol 216 (12), 4073-4090.

20. Neubert, E. et al. (2018) Chromatin swelling drives neutrophil extracellular trap release. Nat Commun 9 (1), 3767.

21. Liu, M.L. (2020) Functional actin cytoskeleton is required in early stage of NETosis induction. Proc Natl Acad Sci U S A 117 (37), 22653-22654.

22. Thiam, H.R. et al. (2020) NETosis proceeds by cytoskeleton and endomembrane disassembly and PAD4-mediated chromatin decondensation and nuclear envelope rupture. Proc Natl Acad Sci U S A 117 (13), 7326-7337.

23. Hall, A. (1998) Rho GTPases and the actin cytoskeleton. Science 279 (5350), 509-14.

24. Rikitake, Y. and Liao, J.K. (2005) Rho GTPases, statins, and nitric oxide. Circ Res 97 (12), 1232-5.

25. Alisafaei, F. et al. (2019) Regulation of nuclear architecture, mechanics, and nucleocytoplasmic shuttling of epigenetic factors by cell geometric constraints. Proc Natl Acad Sci U S A 116 (27), 13200-13209.

26. Somlyo, A.P. and Somlyo, A.V. (2003) Ca2+ sensitivity of smooth muscle and nonmuscle myosin II: modulated by G proteins, kinases, and myosin phosphatase. Physiol Rev 83 (4), 1325-58.

27. Rikitake, Y. et al. (2005) Decreased perivascular fibrosis but not cardiac hypertrophy in ROCK1+/- haploinsufficient mice. Circulation 112 (19), 2959-65.

28. Duran-Struuck, R. and Dysko, R.C. (2009) Principles of bone marrow transplantation (BMT): providing optimal veterinary and husbandry care to irradiated mice in BMT studies. J Am Assoc Lab Anim Sci 48 (1), 11-22.

29. Down, J.D. et al. (1991) Syngeneic and allogeneic bone marrow engraftment after total body irradiation: dependence on dose, dose rate, and fractionation. Blood 77 (3), 661-9.

30. Marino, R. et al. (2013) Delayed marrow infusion in mice enhances hematopoietic and osteopoietic engraftment by facilitating transient expansion of the osteoblastic niche. Biol Blood Marrow Transplant 19 (11), 1566-73.
31. Menke, J. et al. (2008) Sunlight triggers cutaneous lupus through a CSF-1-dependent mechanism in MRL-Fas(lpr) mice. J Immunol 181 (10), 7367-79.
32. Sontheimer, C. et al. (2017) Ultraviolet B Irradiation Causes Stimulator of Interferon Genes-Dependent Production of Protective Type I Interferon in Mouse Skin by Recruited Inflammatory Monocytes. Arthritis Rheumatol 69 (4), 826-836.
33. Cano, M.L. et al. (1992) Mechanisms responsible for F-actin stabilization after lysis of polymorphonuclear leukocytes. J Cell Biol 116 (5), 1123-34.
34. Marathe, G.K. et al. (2005) Ultraviolet B radiation generates platelet-activating factor-like phospholipids underlying cutaneous damage. J Biol Chem 280 (42), 35448-57.
35. Liu, M.L. et al. (2007) Cholesterol enrichment of human monocyte/macrophages induces surface exposure of phosphatidylserine and the release of biologically-active tissue factor-positive microvesicles. Arterioscler Thromb Vasc Biol 27 (2), 430-5.
36. Downey, G.P. et al. (1992) Phorbol ester-induced actin assembly in neutrophils: role of protein kinase C. J Cell Biol 116 (3), 695-706.
37. Yamamura, S. et al. (2020) Yes-associated protein 1 translocation through actin cytoskeleton organization in trophectoderm cells. Dev Biol 468 (1-2), 14-25.
38. Thomas, D.G. et al. (2015) Non-muscle myosin IIB is critical for nuclear translocation during 3D invasion. J Cell Biol 210 (4), 583-94.
39. Chung, C.Y. et al. (2000) Role of Rac in controlling the actin cytoskeleton and chemotaxis in motile cells. Proc Natl Acad Sci U S A 97 (10), 5225-30.

40. Diez, S. et al. (2005) Subsecond reorganization of the actin network in cell motility and chemotaxis. Proc Natl Acad Sci U S A 102 (21), 7601-6.
41. Carlsson, A.E. (2010) Actin dynamics: from nanoscale to microscale. Annu Rev Biophys 39, 91-110.
42. Keller, H.U. et al. (1989) Diacylglycerols and PMA induce actin polymerization and distinct shape changes in lymphocytes: relation to fluid pinocytosis and locomotion. J Cell Sci 93 (Pt 3), 457-65.
43. Gallo, R.M. et al. (2012) Regulation of the actin cytoskeleton by Rho kinase controls antigen presentation by CD1d. J Immunol 189 (4), 1689-98.
44. Wang, H.W. et al. (2008) Deficiency of ROCK1 in bone marrow-derived cells protects against atherosclerosis in LDLR-/- mice. FASEB J 22 (10), 3561-70.
45. Qu, F. et al. (2019) Cell migration: implications for repair and regeneration in joint disease. Nat Rev Rheumatol 15 (3), 167-179.
46. Yang, L. et al. (2020) DNA of neutrophil extracellular traps promotes cancer metastasis via CCDC25. Nature 583 (7814), 133-138.
47. Hofbauer, T.M. et al. (2020) Neutrophil Extracellular Traps Induce MCP-1 at the Culprit Site in ST-Segment Elevation Myocardial Infarction. Front Cell Dev Biol 8, 564169.
48. Roussel, L. et al. (2010) IL-17 promotes p38 MAPK-dependent endothelial activation enhancing neutrophil recruitment to sites of inflammation. J Immunol 184 (8), 4531-7.
49. Smart, S.J. and Casale, T.B. (1994) Pulmonary epithelial cells facilitate TNF-alpha-induced neutrophil chemotaxis. A role for cytokine networking. J Immunol 152 (8), 4087-94.
50. Li, L. et al. (2010) IL-17 produced by neutrophils regulates IFN-gamma-mediated neutrophil migration in mouse kidney ischemia-reperfusion injury. J Clin Invest 120 (1), 331-42.

51. Griffin, G.K. et al. (2012) IL-17 and TNF-alpha sustain neutrophil recruitment during inflammation through synergistic effects on endothelial activation. J Immunol 188 (12), 6287-99.
52. Crow, M.K. (2014) Type I interferon in the pathogenesis of lupus. J Immunol 192 (12), 5459-68.
53. Crow, M.K. et al. (2018) Type I Interferons in Autoimmune Disease. Annu Rev Pathol.
54. Hilda, J.N. and Das, S.D. (2016) TLR stimulation of human neutrophils lead to increased release of MCP-1, MIP-1alpha, IL-1beta, IL-8 and TNF during tuberculosis. Hum Immunol 77 (1), 63-67.
55. Yamada, M. et al. (2011) Interferon-gamma production by neutrophils during bacterial pneumonia in mice. Am J Respir Crit Care Med 183 (10), 1391-401.
56. Lindau, D. et al. (2013) TLR9 independent interferon alpha production by neutrophils on NETosis in response to circulating chromatin, a key lupus autoantigen. Ann Rheum Dis.
57. Agak, G.W. et al. (2021) Extracellular traps released by antimicrobial TH17 cells contribute to host defense. J Clin Invest 131 (2).
58. Farley, K. et al. (2012) A serpinB1 regulatory mechanism is essential for restricting neutrophil extracellular trap generation. J Immunol 189 (9), 4574-81.
59. Shipman, W.D. et al. (2018) A protective Langerhans cell-keratinocyte axis that is dysfunctional in photosensitivity. Sci Transl Med 10 (454).
60. Wolf, S.J. et al. (2018) Human and Murine Evidence for Mechanisms Driving Autoimmune Photosensitivity. Front Immunol 9, 2430.
61. Ongusaha, P.P. et al. (2008) Identification of ROCK1 as an upstream activator of the JIP-3 to JNK signaling axis in response to UVB damage. Sci Signal 1 (47), ra14.

62. Colonna, L. et al. (2014) Beyond apoptosis in lupus. Curr Opin Rheumatol 26 (5), 459-66.
63. Sim, J.H. et al. (2021) Immune Cell-Stromal Circuitry in Lupus Photosensitivity. J Immunol 206 (2), 302-309.
64. Zawrotniak, M. et al. (2019) UVA and UVB radiation induce the formation of neutrophil extracellular traps by human polymorphonuclear cells. J Photochem Photobiol B 196, 111511.
65. Yipp, B.G. and Kubes, P. (2013) NETosis: how vital is it? Blood 122 (16), 2784-94.
66. Papayannopoulos, V. (2018) Neutrophil extracellular traps in immunity and disease. Nat Rev Immunol 18 (2).
67. Boeltz, S. et al. (2019) To NET or not to NET:current opinions and state of the science regarding the formation of neutrophil extracellular traps. Cell Death Differ 26 (3), 395-408.
68. Fuchs, T.A. et al. (2007) Novel cell death program leads to neutrophil extracellular traps. J Cell Biol 176 (2), 231-41.
69. Halverson, T.W. et al. (2015) DNA is an antimicrobial component of neutrophil extracellular traps. PLoS Pathog 11 (1), e1004593.
70. Yang, H. et al. (2016) New Insights into Neutrophil Extracellular Traps: Mechanisms of Formation and Role in Inflammation. Front Immunol 7, 302.
71. Neubert, E. et al. (2020) The power from within - understanding the driving forces of neutrophil extracellular trap formation. J Cell Sci 133 (5).
72. Thiam, H.R. et al. (2020) Cellular Mechanisms of NETosis. Annu Rev Cell Dev Biol 36, 191-218.
73. Matoba, K. et al. (2014) Rho-kinase regulation of TNF-alpha-induced nuclear translocation of NF-kappaB RelA/p65 and M-CSF expression via p38 MAPK in mesangial cells. Am J Physiol Renal Physiol 307 (5), F571-80.

74. Wesolowska, N. et al. (2020) Actin assembly ruptures the nuclear envelope by prying the lamina away from nuclear pores and nuclear membranes in starfish oocytes. Elife 9.
75. Chugh, P. and Paluch, E.K. (2018) The actin cortex at a glance. J Cell Sci 131 (14).
76. Papagoras, C. et al. (2021) IL-17A expressed on neutrophil extracellular traps promotes mesenchymal stem cell differentiation toward bone-forming cells in ankylosing spondylitis. Eur J Immunol 51 (4), 930-942.
77. Cheng, C.I. et al. (2015) High glucose activates Raw264.7 macrophages through RhoA kinase-mediated signaling pathway. Cell Signal 27 (2), 283-92.
78. Wang, C. et al. (2015) Inhibition of the Rho/Rho kinase pathway prevents lipopolysaccharide-induced hyperalgesia and the release of TNF-alpha and IL-1beta in the mouse spinal cord. Sci Rep 5, 14553.
79. Biswas, P.S. et al. (2010) Phosphorylation of IRF4 by ROCK2 regulates IL-17 and IL-21 production and the development of autoimmunity in mice. J Clin Invest 120 (9), 3280-95.
80. Zanin-Zhorov, A. et al. (2014) Selective oral ROCK2 inhibitor down-regulates IL-21 and IL-17 secretion in human T cells via STAT3-dependent mechanism. Proc Natl Acad Sci U S A 111 (47), 16814-9.
81. Sharma, M.R. et al. (2020) Effect of TNFalpha blockade on UVB-induced inflammatory cell migration and collagen loss in mice. J Photochem Photobiol B 213, 112072.
82. Yang, D. et al. (2000) LL-37, the neutrophil granule- and epithelial cell-derived cathelicidin, utilizes formyl peptide receptor-like 1 (FPRL1) as a receptor to chemoattract human peripheral blood neutrophils, monocytes, and T cells. J Exp Med 192 (7), 1069-74.

83. Kurosaka, K. et al. (2005) Mouse cathelin-related antimicrobial peptide chemoattracts leukocytes using formyl peptide receptor-like 1/mouse formyl peptide receptor-like 2 as the receptor and acts as an immune adjuvant. J Immunol 174 (10), 6257-65.
84. Skopelja-Gardner, S. et al. (2020) The early local and systemic Type I interferon responses to ultraviolet B light exposure are cGAS dependent. Sci Rep 10 (1), 7908.
85. Seery, J.P. (2000) IFN-gamma transgenic mice: clues to the pathogenesis of systemic lupus erythematosus? Arthritis Res 2 (6), 437-440.
86. Sarkar, M.K. et al. (2018) Photosensitivity and type I IFN responses in cutaneous lupus are driven by epidermal-derived interferon kappa. Ann Rheum Dis.
87. Oke, V. et al. (2019) High levels of circulating interferons type I, type II and type III associate with distinct clinical features of active systemic lupus erythematosus. Arthritis Res Ther 21 (1), 107.
88. Isgro, J. et al. (2013) Enhanced rho-associated protein kinase activation in patients with systemic lupus erythematosus. Arthritis Rheum 65 (6), 1592-602.
89. Rozo, C. et al. (2016) Targeting the RhoA-ROCK pathway to reverse T-cell dysfunction in SLE. Ann Rheum Dis 76 (4), 740-747.

Figure Legends

Figure 1. Disruption of actin cytoskeleton or actomyosin cytoskeletal networks attenuated NETosis in neutrophils. **A**,**B**. dPMNs (**A**) or primary human neutrophils from different healthy donors (**B**) were exposed to 50 nM PMA for 3h without or with 30 min pretreatment by 10 μM Cytochalasin D (Cyto D), 50 μM Blebbistatin, or 1 μM ML7, then detection of NETosis with Sytox Green staining by microplate reader. **C**. Primary bone marrow (BM) mouse neutrophils from different C57BL/6 wild type (WT) mice were treated with 10 μM PAF (a physiological stimulus) for 3h, without or with 30 min pretreatment by 10 μM Cyto D, 50 μM Blebbistatin, or 1 μM ML7, and stained by cell permeable SYTO Red and cell impermeable Sytox Green, then detected by fluorescent microscopy (**C**). Images were taken by confocal microscopy, followed by automated quantification of NETs in 5-6 non-overlapping areas per well using ImageJ for calculation of % cells with NET formation. **D-F**. Representative images and summary analysis for the effects of Cyto D, Blebbistatin, and ML7 on nuclear translocation of PKCα and nuclear lamina (lamin B) disintegration in dPMNs exposed to 50 nM PMA for 1h without or with pretreatment by above inhibitors. All cells were stained for **lamin B** and **PKCα** with corresponding antibodies. Scale bars, 10 μm. **G.** Schematic illustration of the involvement of actin cytoskeleton and actomyosin cytoskeletal networks, and their corresponding inhibitors in NETosis. All results in panels A-C represent 5-6 biological replicates. Panels E-F were summary analyses of at least 10 cells of each conditions from three independent experiments. For sample sets with normal distribution, ANOVA analysis with post hoc Student-Newman Keuls test were conducted. Panels **A-C,E,F** display means±SD.

Figure 2. PKCα nuclear translocation and actin cytoskeleton assembly were regulated by Rho kinase 1 (ROCK1). **A.** Representative images for the time course study of PKCα nuclear translocation, subsequent lamin B disassembly and nuclear lamina disintegration, and NET release in dPMNs exposed to 50 nM PMA for 0-180 min, then stained simultaneously for **DNA**, **lamin B** (probed by primary anti-lamin B, and FITC-labeled secondary antibody), and **PKCα** (primary anti-PKCα, and PE-labeled secondary antibody) under confocal fluorescent microscopy. Scale bars, 10 μm. **B-C**. Summary analyses of panel A for cellular distribution of both cytosolic (B) and nuclear (C) PKCα in dPMNs treated with 50 nM PMA for 0-60 min. For 0 min at panels A-C, analysis started after 5 min of PMA stimulation to allow the suspension dPMNs to adhere in order to compare with the adherent dPMNs at later time points for microscopic analysis. **D-E**. Representative flow cytometry histograms and summary analyses for the time course of F-actin polymerization in dPMNs exposed to 50 nM PMA for 0-180 min, the pemeabilized cells were probed with phalloidin-RFP. **F**. Time course of ROCK activation in dPMNs exposed to 50 nM PMA for 0-180 min, detected by ROCK activity ELISA. **G-H**. Representative and summary analyses of F-actin polymerization in WT primary mouse neutrophils stimulated by 50 nM PMA for 0 or 60 min, and PMA treatment at 60 min without or with pretreatment by 50 μM ROCK inhibitors Y27632 for 30 min. **I-J**. Representative and summary analyses of F-actin polymerization in mouse neutrophils from WT or $ROCK^{+/-}$ mice stimulated without or with 50 nM PMA for 60 min. Cells in panels G-J were detected by flow cytometry by staining with phalloidin-FITC and anti-ly6G-PE. **K**. Representative images for the effect of ROCK inhibition on PKCα nuclear translocation and nuclear envelope disintegration in dPMNs exposed to PMA for 60 min without or with pretreatment by ROCK inhibitors, control cells same as 0 min in panels A-C. All cells were stained for **lamin B** and **PKCα** with their corresponding Abs. Scale bar, 10 μm. Light blue arrows

in panels A,K indicate the disintegration/rupture of nuclear lamina at 60 min after PMA treatment, while white arrows in panel A indicate the rupture site of the nuclear envelope where the decondensed chromatin released for NET formation at later time points. Panels B-C were summary analyses of at least 10 cells at each time point (5-60 min) from three independent experiments. The results of summary anslyses represent 3 (E), 4 (F), or 5 (H,J) biological replicates. For non-normal distributed data (E), Kruskall-Wallis analysis and Dunn´s post-hoc test for pairwise comparisons were conducted. For sample sets with normal distribution (B,C,F,H,J), ANOVA analysis with post hoc Student-Newman Keuls test were conducted. In panels B,C,F, P**<0.01 or P***<0.001 vs 0 min, $P^{\dagger\dagger\dagger}$<0.01 vs 60 min. Panels B,C,E,F,H,J display means±SD as indicated.

Figure 3. Inhibition of ROCK1 attenuated NETosis in neutrophils. Panels **A,B** show the results of NETosis of either dPMNs (**A**) or primary human neutrophils from different healthy donors (**B**), which were exposed to 50 nM PMA for 3h without or with 30min pretreatment by 50 μM ROCK inhibitors (Y27632, HA1077, AS1892802), then detection of NET formation by microplate reader. **C**-**E**, Summary analysis (**C**-**D**) and (**E**) representative of NET formation of mouse BM neutrophils from WT mice without or with pretreatment by different ROCK inhibitors (**C**), or BM neutrophils from WT vs $ROCK1^{+/-}$ mice (**D-E**), and stimulated without or with 10 μM PAF (**C**,**D**,**E**) for 3h, and stained with SYTO Red and Sytox Green. Images were taken by fluorescent microscopy, and % cells with NET formation was analyzed as described in Fig 1. All results represent 5 or 6 biological replicates. Panel E represent images of the replicates (D). Scale bars, 100μm. Panels A-D display mean±SD. For non-normal distributed data (D), Kruskall-Wallis analysis and Dunn´s post-hoc test were conducted. For sample sets with normal distribution (A-C), ANOVA analysis with post hoc Student-Newman Keuls test for pairwise comparisons was conducted.

Figure 4. Hematopoietic-specific ROCK1 deficiency protected mice from UVB-induced skin inflammation in BMT-ROCK1$^{+/-}$ mice. **A-E**. Representative H&E staining images (A) and summary analysis of the thickness of epidermis and dermis (B,C), infiltration of inflammatory (nucleated) cells in the dermis and subcutis (D) and their correlation with dermis thickness (E) based on H&E staining of skin sections of BMT-WT vs BMT-ROCK1$^{+/-}$ mice that were irradiated without (sham) or with UVB. **F-H.** Representative images (F) and summary analysis of NETosis (G), and its correlation with skin thickness (H) in skin of BMT-WT vs BMT-ROCK1$^{+/-}$ mice that were irradiated without (sham) or with UVB. **I**. Relative migration analysis of BM neutrophils of WT vs ROCK1$^{+/-}$ mice was conducted with Boyden chamber by stimulation without or with CXCL1. **J**. Neutrophil infiltration per unit area in skin of UVB-irradiated BMT-WT vs BMT-ROCK1$^{+/-}$ mice. **K**. Percentage of NETotic cells among neutrophils in skin of UVB-irradiated BMT-WT vs BMT-ROCK1$^{+/-}$ mice. For panels F-H,J,K, skin sections were stained by antibodies against **Ly6G** (PE) neutrophil marker, citrullinated histone H3 (**citH3**, FITC), and **DAPI** for DNA. In panels A,F, Scale bars, 100 μm. All results represent 4-8 biological replicates as indicated in individual panels. For non-normal distributed data sets (B), Kruskall-Wallis analysis and Dunn´s post-hoc pairwise comparisons were conducted. For sample sets with normal distribution (C,D,G,I,J,K), multiple comparisons were conducted by ANOVA analysis with Student-Newman Keuls post hoc pairwise comparisons, while student's t-test were conducted for two groups comparisons (J,K).

Figure 5. Hematopoietic-specific ROCK1 deficiency attenuated skin inflammation with decreased exhibition of NET-associated pro-inflammatory cytokines in UVB-irradiated BMT-ROCK1$^{+/-}$

mice. **A-I**. Summary analyses (**A**,**D**,**F**,**H**) and representative images (**B**,**C**,**E**,**G**,**I**) of skin sections of BMT-WT vs BMT-ROCK1$^{+/-}$ mice that were irradiated without (sham) or with UVB, and stained by PE-conjugated rat anti-mouse **Ly6G** Ab, and FITC labeled rat anti-mouse **IL-17A**, **TNFα**, **IFNγ**, or **IFNα**. DNA was stained by **DAPI** for panels **A-I**. Yellow arrows indicate NETotic neutrophils, and white arrows show non-netting neutrophils in panels B,C,E,G,I. Scale bars, 100μm. All results represent 4-7 biological replicates as indicated in individual panels (A,D,F,H). For non-normal distributed data sets (A,F), Kruskall-Wallis analysis and Dunn´s post-hoc pairwise comparisons were conducted. For sample sets with normal distribution (D,H), multiple comparisons were conducted by ANOVA analysis with Student-Newman Keuls post hoc pairwise comparisons.

Figure 6. Genetic deficiency of ROCK1 decreased formation of NETs and attenuated their display of pro-inflammatory cytokines in neutrophils from ROCK1 deficient mice. **A-L**. Summary flow cytometry analyses (**A**,**D**,**G,J**), representative fluorescent images (**B**,**E**,**H,K**) and their summary analyses (**C**,**F**,**I**,**L**) of BM neutrophils from ROCK1$^{+/-}$ mice or their WT littermates were treated without or with 10 μM PAF (for IFNα induction in **J-L**, treatment with PAF and isolated NETs from cultured neutrophils of MRL/lpr mice) for 20h, followed by fixation, permeabilization, and staining of neutrophils by PE-conjugated anti-mouse **Ly6G**, FITC labeled anti-mouse **IL-17A**, **TNFα**, **IFNγ**, **or IFNα**, then following by flow cytometry or confocal microscopy analyses. DNA was stained by **DAPI.** Scale bars, 50μm. Arrows indicate NETs with extracellular display of different cytokines. All results represent 4-9 biological replicates as indicated in individual panels. All sample sets with normal distribution, the multiple comparisons were conducted by ANOVA analysis with Student-Newman Keuls post hoc tests.

Figure 1.

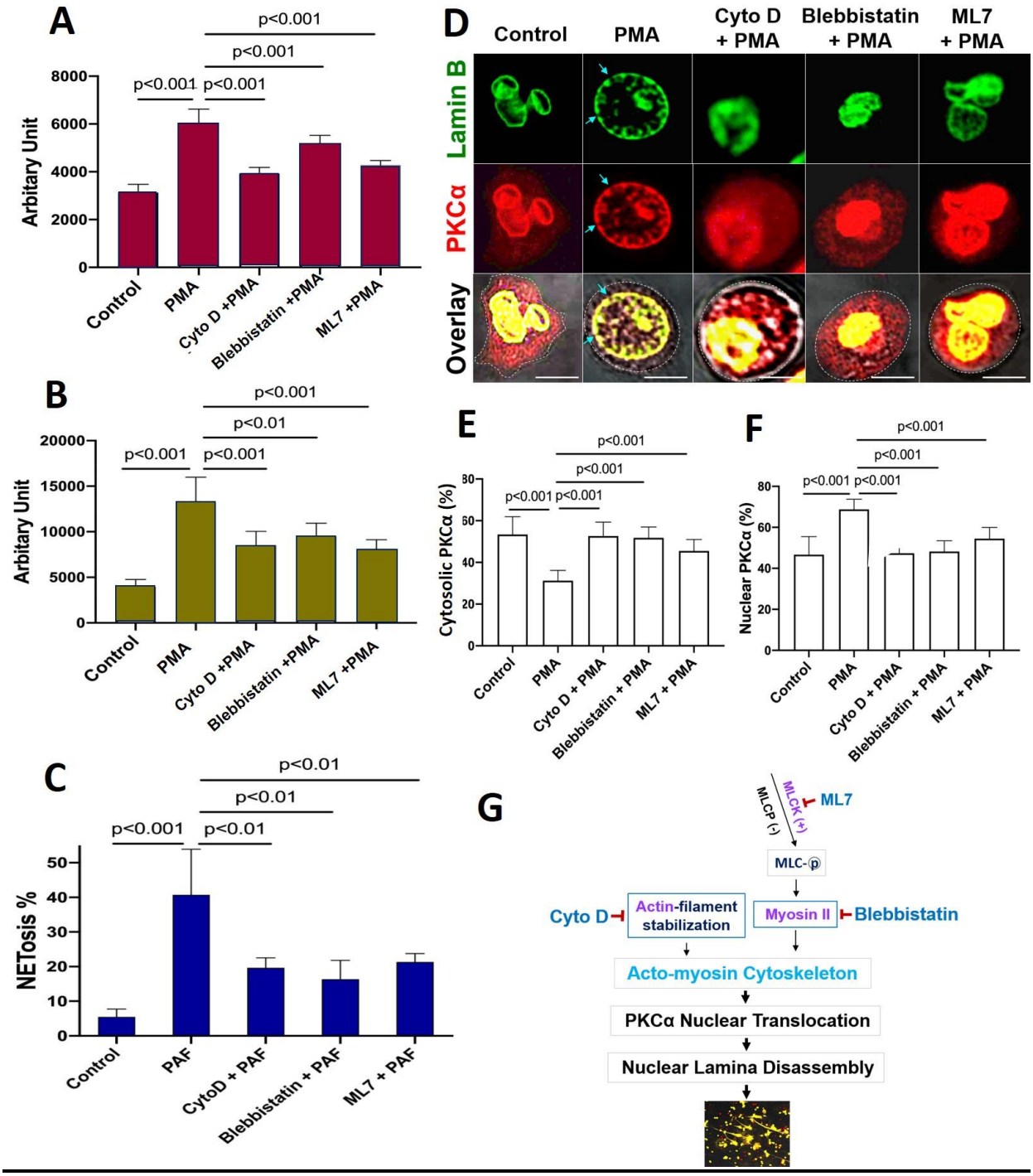
A
p<0.001
p<0.001
p<0.001
p<0.001
Arbitary Unit
8000
6000
4000
2000
0
Control
PMA
Cyto D +PMA
Blebbistatin +PMA
ML7 +PMA
B
p<0.001
p<0.01
p<0.001
p<0.001
Arbitary Unit
20000
15000
10000
5000
0
Control
PMA
Cyto D +PMA
Blebbistatin +PMA
ML7 +PMA
C
p<0.01
p<0.01
p<0.001
p<0.01
NETosis %
50
40
30
20
10
0
Control
PAF
CytoD + PAF
Blebbistatin + PAF
ML7 + PAF
D
Control
PMA
Cyto D + PMA
Blebbistatin + PMA
ML7 + PMA
Lamin B
PKCα
Overlay
E
p<0.001
p<0.001
p<0.001
p<0.001
Cytosolic PKCα (%)
80
60
40
20
0
Control
PMA
Cyto D + PMA
Blebbistatin + PMA
ML7 + PMA
F
p<0.001
p<0.001
p<0.001
p<0.001
Nuclear PKCα (%)
80
60
40
20
0
Control
PMA
Cyto D + PMA
Blebbistatin + PMA
ML7 + PMA
G
MLCP (-)
MLCK (+)
ML7
MLC-ⓟ
Cyto D
Actin-filament stabilization
Myosin II
Blebbistatin
Acto-myosin Cytoskeleton
PKCα Nuclear Translocation
Nuclear Lamina Disassembly

Figure 2.

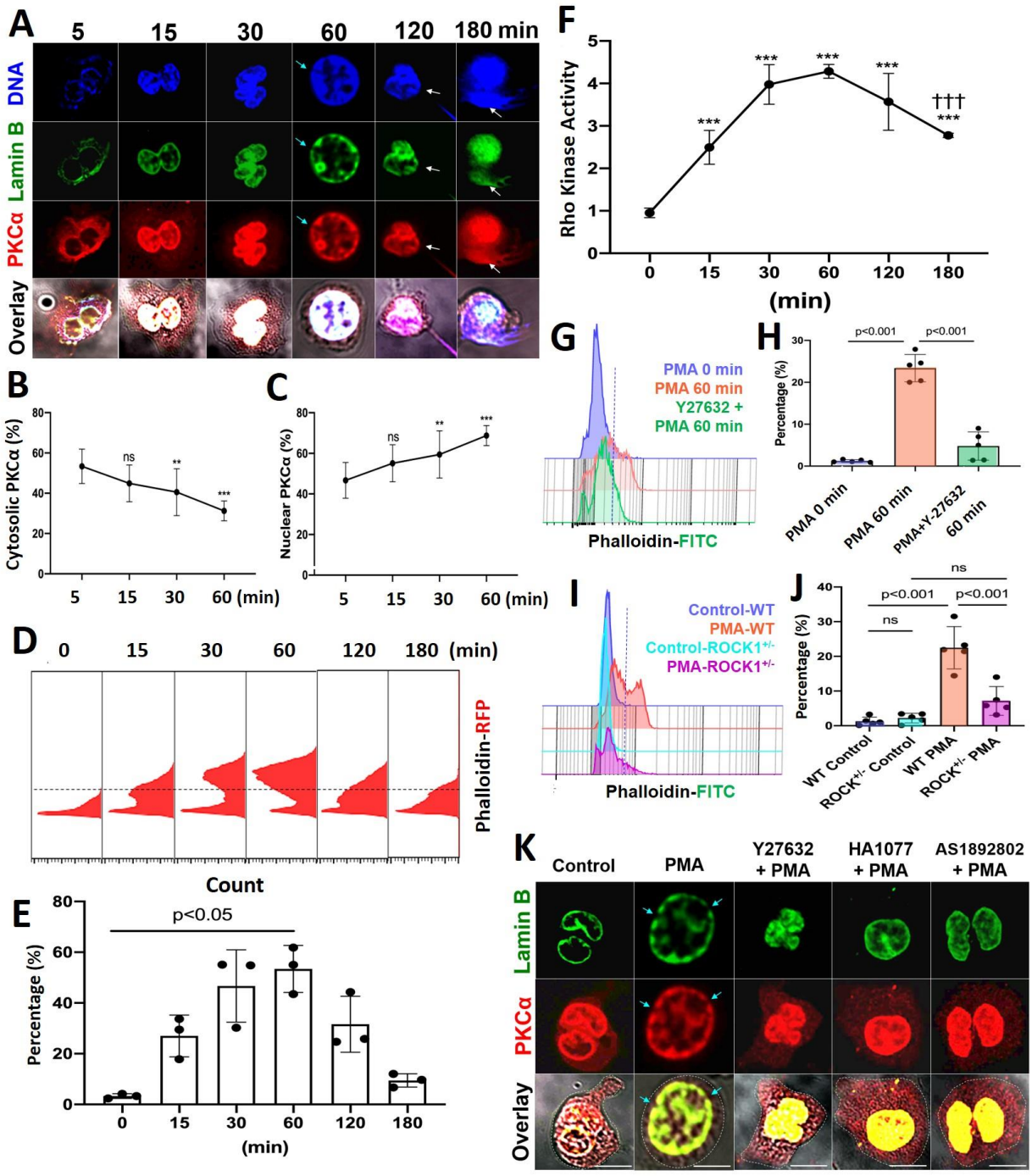
A
5
15
30
60
120
180 min
DNA
Lamin B
PKCα
Overlay
B
Cytosolic PKCα (%)
ns
**
***
5
15
30
60 (min)
C
Nuclear PKCα (%)
ns
**
***
5
15
30
60 (min)
D
0
15
30
60
120
180 (min)
Phalloidin-RFP
Count
E
p<0.05
Percentage (%)
0
15
30
60
120
180
(min)
F
Rho Kinase Activity
***
***
***
***
†††
0
15
30
60
120
180
(min)
G
PMA 0 min
PMA 60 min
Y27632 +
PMA 60 min
Phalloidin-FITC
H
p<0.001
p<0.001
Percentage (%)
PMA 0 min
PMA 60 min
PMA+Y-27632
60 min
I
Control-WT
PMA-WT
Control-ROCK1+/-
PMA-ROCK1+/-
Phalloidin-FITC
J
ns
p<0.001
p<0.001
ns
Percentage (%)
WT Control
ROCK+/- Control
WT PMA
ROCK+/- PMA
K
Control
PMA
Y27632
+ PMA
HA1077
+ PMA
AS1892802
+ PMA
Lamin B
PKCα
Overlay

Figure 3.

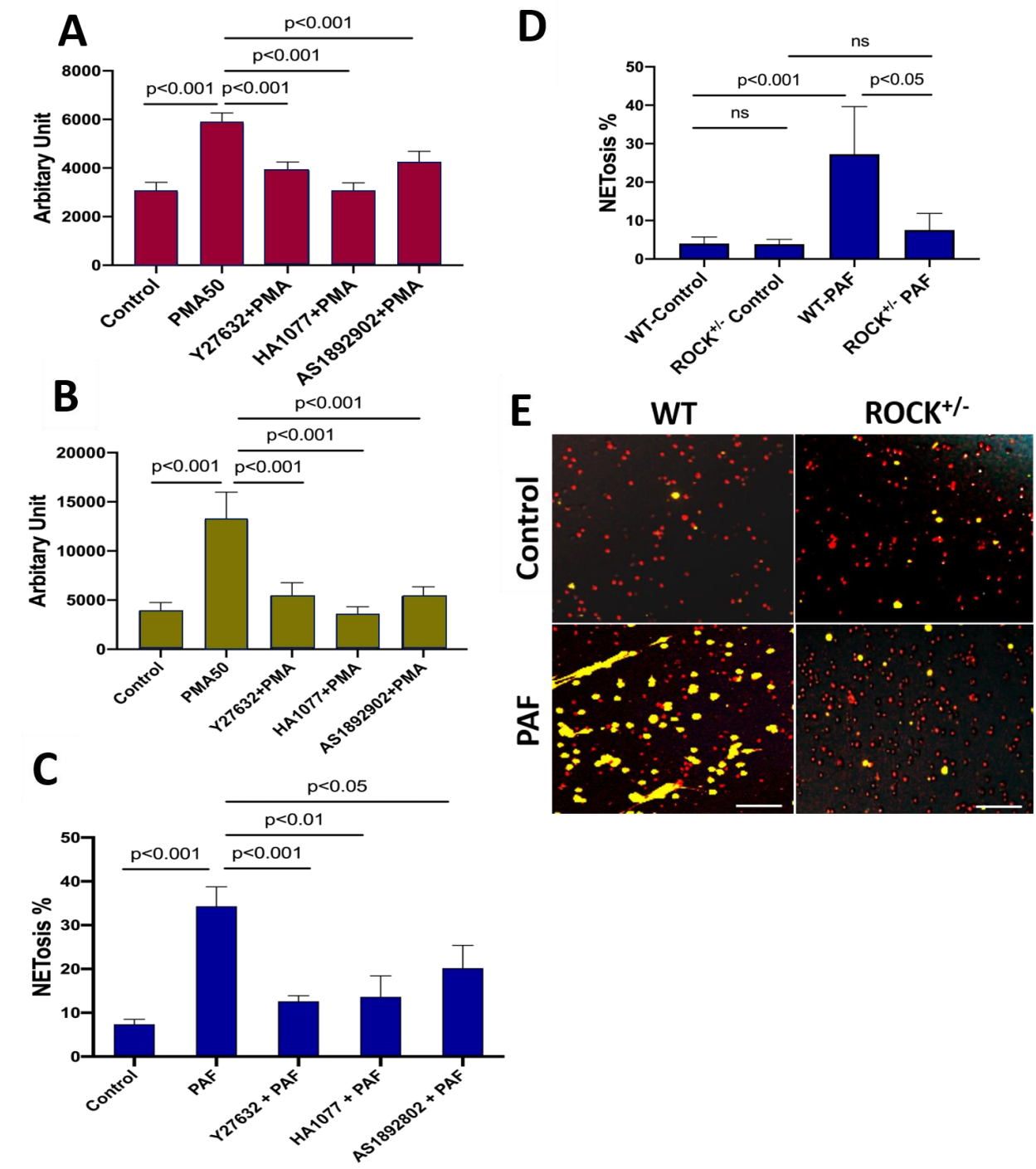
A
p<0.001
p<0.001
p<0.001
p<0.001
Arbitary Unit
8000
6000
4000
2000
0
Control
PMA50
Y27632+PMA
HA1077+PMA
AS1892902+PMA
B
p<0.001
p<0.001
p<0.001
p<0.001
Arbitary Unit
20000
15000
10000
5000
0
Control
PMA50
Y27632+PMA
HA1077+PMA
AS1892902+PMA
C
p<0.05
p<0.01
p<0.001
p<0.001
NETosis %
50
40
30
20
10
0
Control
PAF
Y27632 + PAF
HA1077 + PAF
AS1892802 + PAF
D
ns
p<0.001
p<0.05
ns
NETosis %
50
40
30
20
10
0
WT-Control
ROCK+/- Control
WT-PAF
ROCK+/- PAF
E
WT
ROCK+/-
Control
PAF

Figure 4.

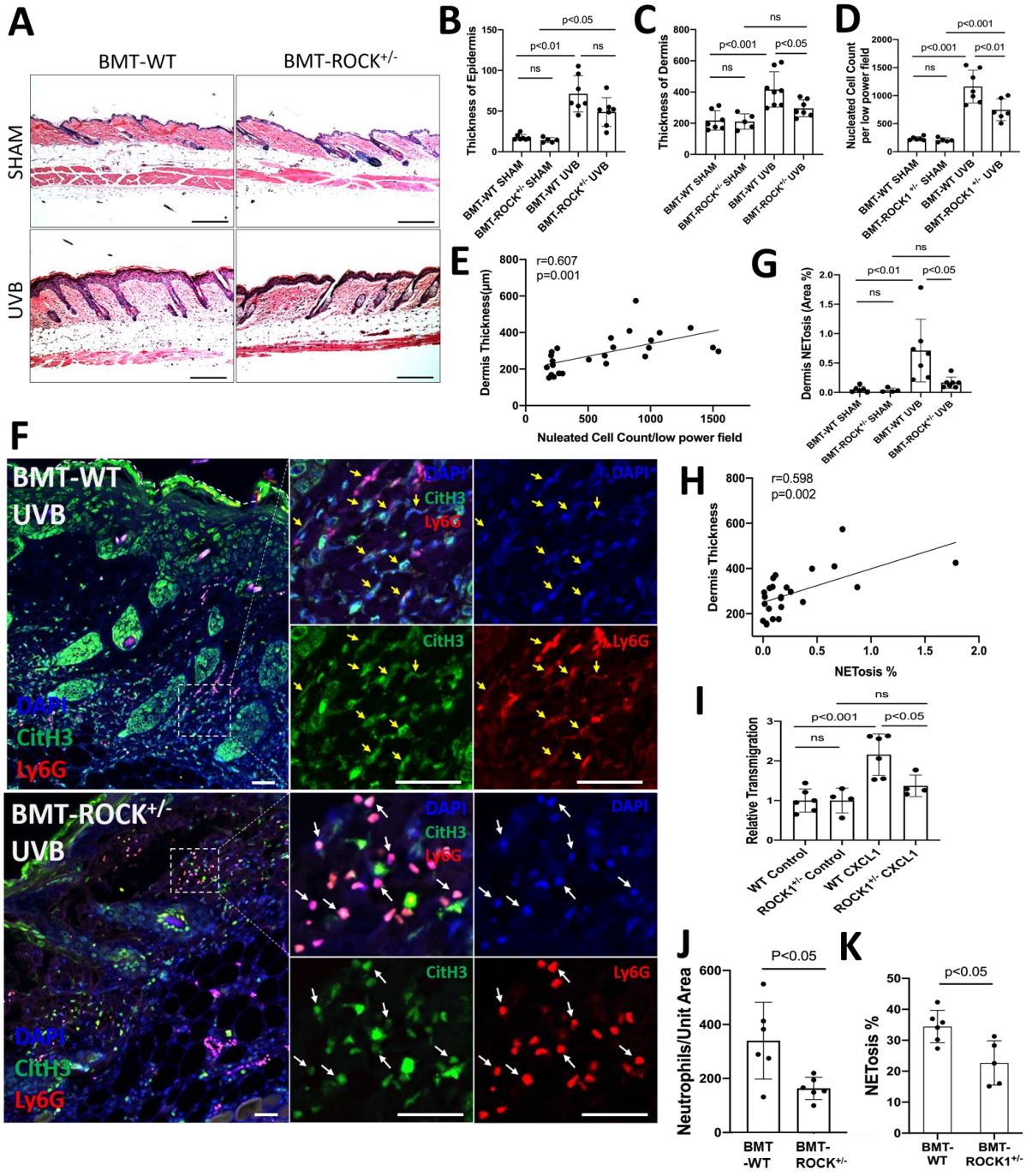
A
BMT-WT
BMT-ROCK+/-
SHAM
UVB
B
Thickness of Epidermis
p<0.05
p<0.01
ns
ns
BMT-WT SHAM
BMT-ROCK+/- SHAM
BMT-WT UVB
BMT-ROCK+/- UVB
C
Thickness of Dermis
ns
p<0.001
p<0.05
ns
D
Nucleated Cell Count per low power field
p<0.001
p<0.001
p<0.01
ns
BMT-ROCK1 +/- SHAM
BMT-ROCK1 +/- UVB
E
r=0.607
p=0.001
Dermis Thickness(µm)
Nuleated Cell Count/low power field
G
Dermis NETosis (Area %)
p<0.01
p<0.05
ns
F
BMT-WT
UVB
DAPI
CitH3
Ly6G
BMT-ROCK+/-
UVB
H
r=0.598
p=0.002
Dermis Thickness
NETosis %
I
Relative Transmigration
p<0.001
p<0.05
ns
ns
WT Control
ROCK1+/- Control
WT CXCL1
ROCK1+/- CXCL1
J
Neutrophils/Unit Area
P<0.05
BMT -WT
BMT-ROCK+/-
K
NETosis %
p<0.05
BMT-WT
BMT-ROCK1+/-

Figure 5.

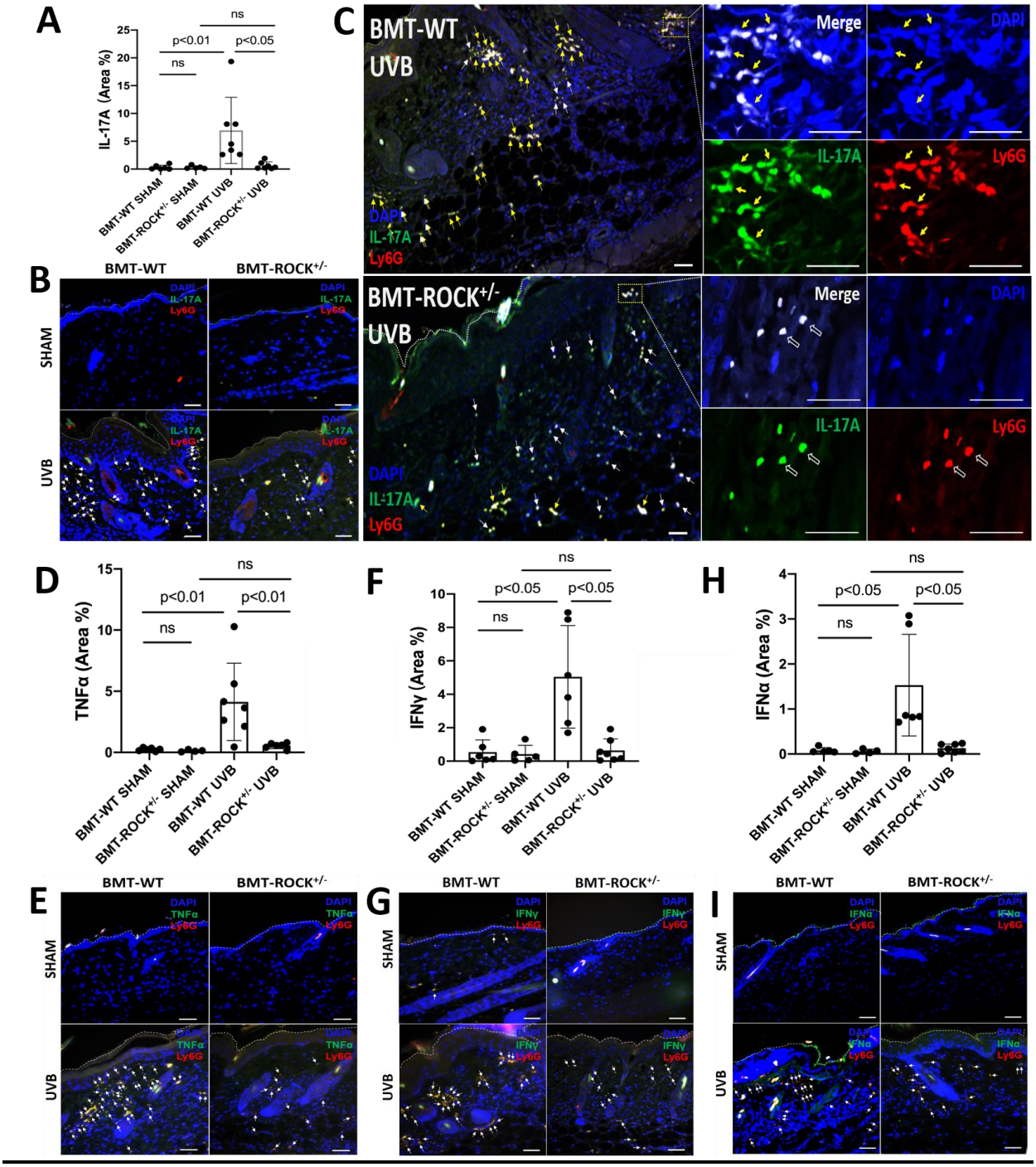
A
IL-17A (Area %)
ns
p<0.01
p<0.05
ns
BMT-WT SHAM
BMT-ROCK+/- SHAM
BMT-WT UVB
BMT-ROCK+/- UVB
B
BMT-WT
BMT-ROCK+/-
SHAM
UVB
DAPI
IL-17A
Ly6G
C
BMT-WT
UVB
BMT-ROCK+/-
UVB
Merge
DAPI
IL-17A
Ly6G
D
TNFα (Area %)
p<0.01
p<0.01
ns
ns
E
TNFα
F
IFNγ (Area %)
p<0.05
p<0.05
ns
ns
G
IFNγ
H
IFNα (Area %)
p<0.05
p<0.05
ns
ns
I
IFNα

Fig 6.

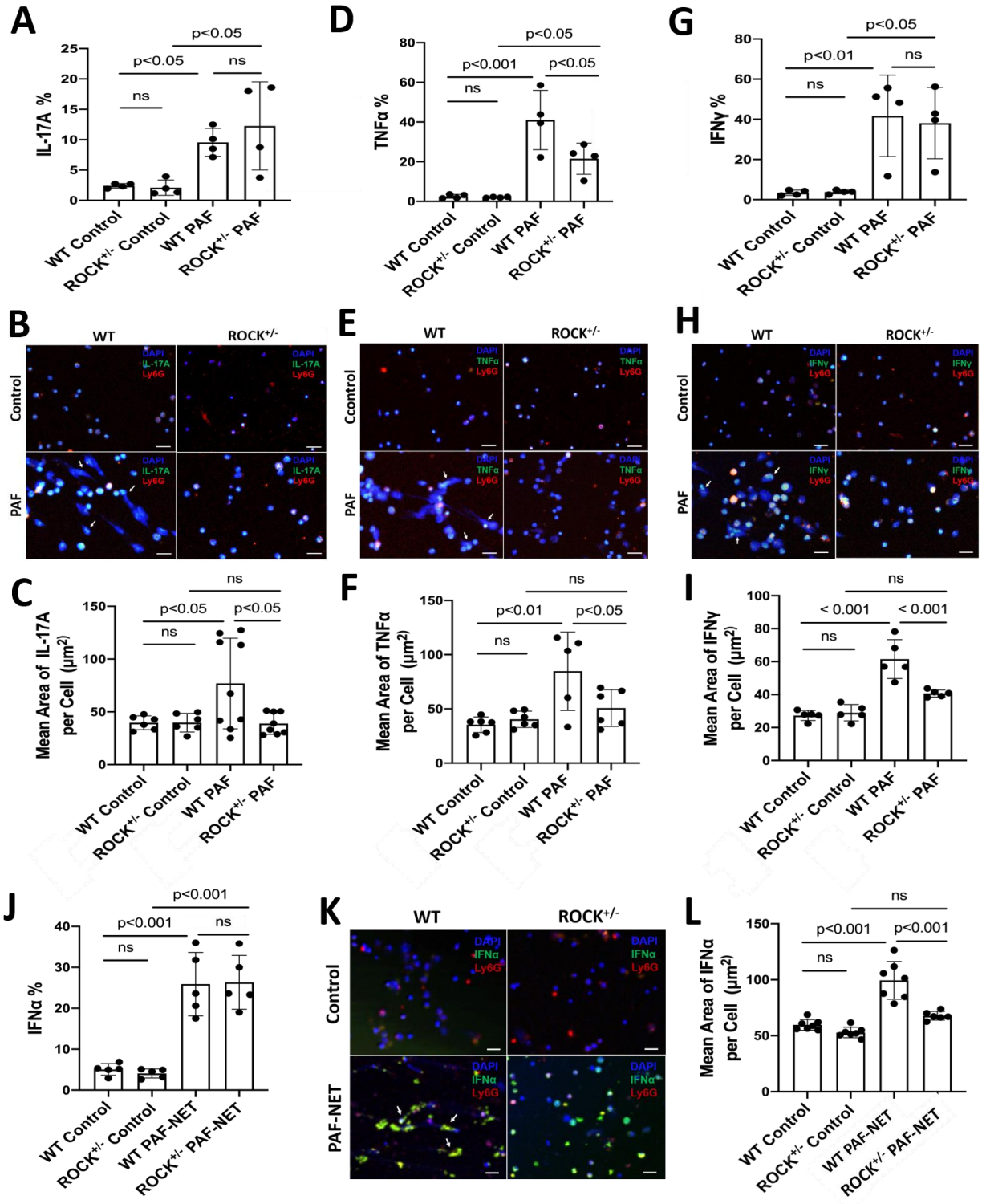
A
IL-17A %
p<0.05
p<0.05
ns
ns
WT Control
ROCK+/- Control
WT PAF
ROCK+/- PAF
D
TNFα %
p<0.05
p<0.001
p<0.05
ns
G
IFNγ %
p<0.05
p<0.01
ns
ns
B
WT
ROCK+/-
Control
PAF
DAPI
IL-17A
Ly6G
E
Ccontrol
TNFα
H
IFNγ
C
Mean Area of IL-17A per Cell (μm2)
ns
p<0.05
p<0.05
ns
F
Mean Area of TNFα per Cell (μm2)
ns
p<0.01
p<0.05
ns
I
Mean Area of IFNγ per Cell (μm2)
ns
< 0.001
< 0.001
ns
J
IFNα %
p<0.001
p<0.001
ns
ns
WT PAF-NET
ROCK+/- PAF-NET
K
IFNα
PAF-NET
L
Mean Area of IFNα per Cell (μm2)
ns
p<0.001
p<0.001
ns

Supplemental Materials

Rho Kinase regulates neutrophil NET formation that is involved in UVB-induced skin inflammation

Running title: ***Rho kinase and NETosis***

Key words: ***Rho kinase, Neutrophil, NETosis, UVB, Skin inflammation.***

Supplemental Figures

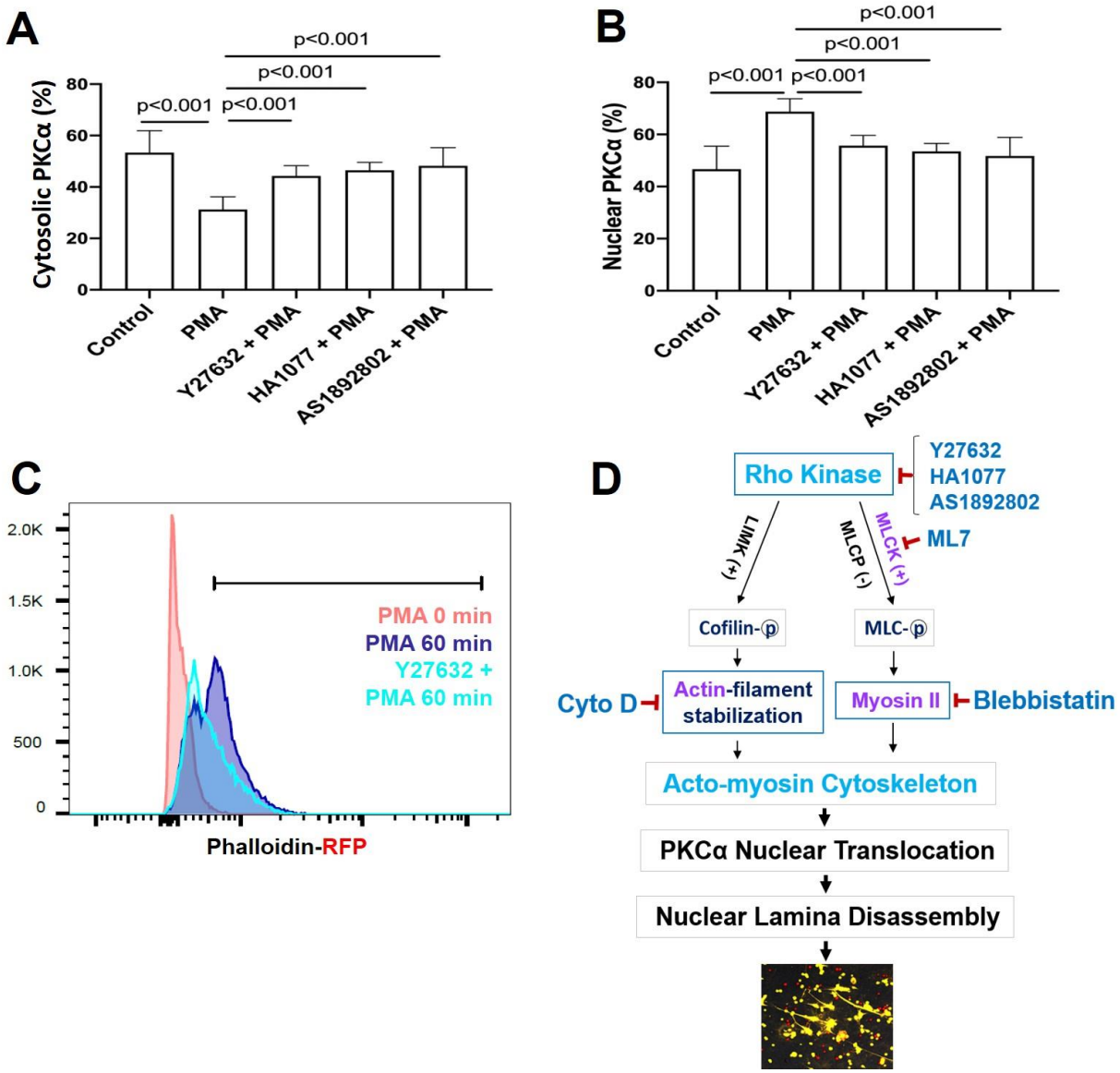

Supplemental Fig 1. A,B. Summary analyses of time course study of PKCα distribution in cytosolic (A) vs nucleus (B) in dPMNs treated by 50 nM PMA for 60 min, then stained for PKCα (primary anti-PKCα, and PE-labeled secondary antibody) and lamin B (primary anti-lamin B, and FITC-labeled secondary antibody), following by confocal fluorescent microscopy, and Image J analyses. **C**. Representative analysis of F-actin polymerization detected by phalloidin-RFP with flow cytometry in dPMNs stimulated by 50 nM PMA for 60 min without or with pretreatment by 50 μM Y27632, ROCK inhibitors for 30 min. **D**. Schematic illustration of the involvement of actin cytoskeleton, actomyosin cytoskeletal networks, their upstream signaling pathways, and ROCK, as well as their corresponding inhibitors in NETosis.

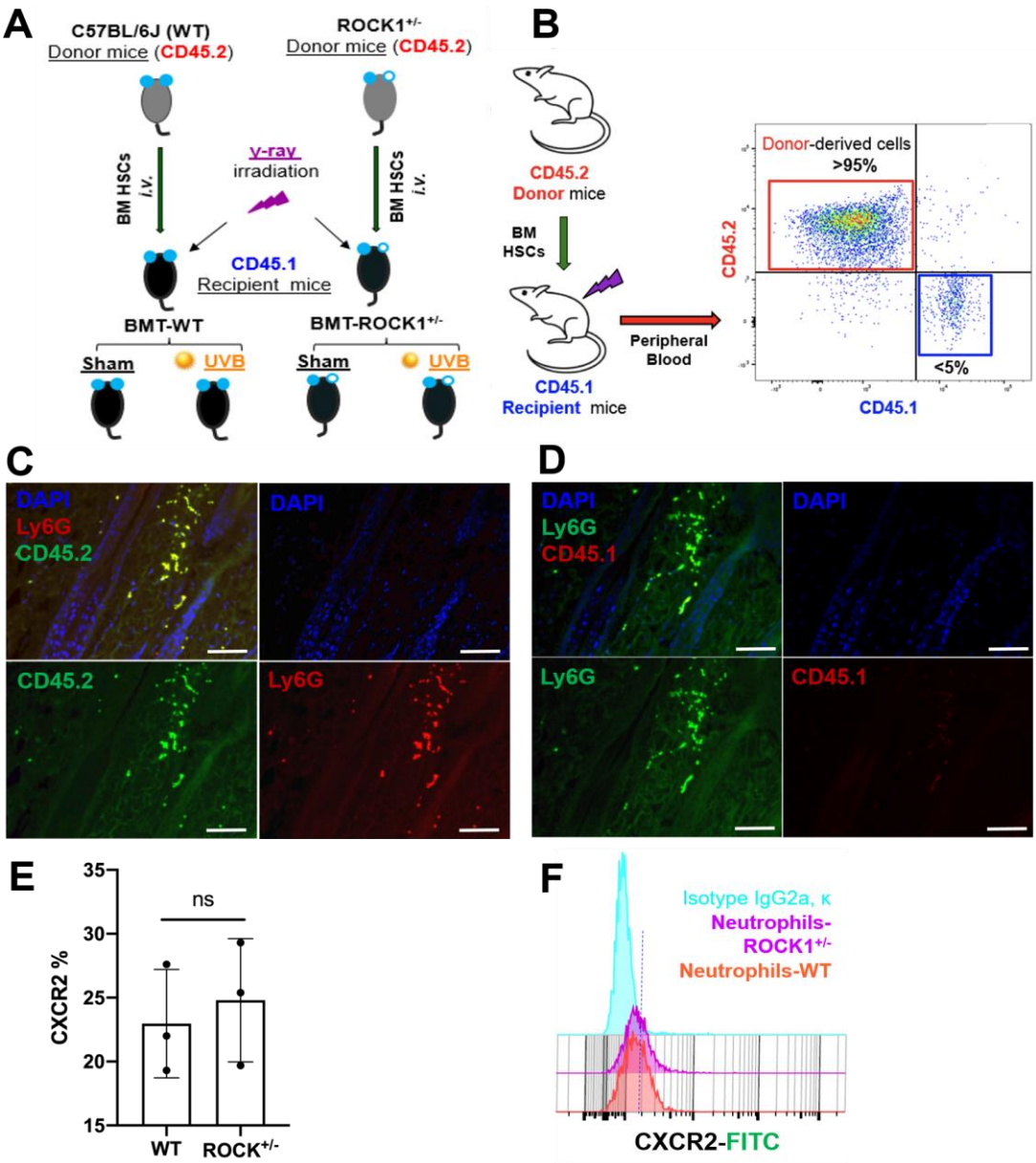

Supplemental Fig 2. A. Experimental design of the BMT-WT and BMT-ROCK1$^{+/-}$ mice that were irradiated without or with UVB. **B.** Representative dot plots of flow cytometry analysis of all BMT experimental mice for detection of reconstitution rate of donor-derived cells (CD45.2) in peripheral blood of recipient mice (CD45.1). **C**,**D**. Representative images of immunohistochemistry staining of skin lesions from UVB-irradiated CD45.1 recipient mice with BMT of HSCs from WT donors, stained by antibodies against **Ly6G** (PE) and **CD45.2** (FITC) (**C**), or antibodies against **CD45.1** (PE) and **LY6G** (FITC) (**D**), and **DAPI** for DNA. **E**,**F**. Summary analyses and representative histograms of flow cytometry analyses of CXCR2 expression in BM neutrophils from WT vs ROCK1$^{+/-}$ mice, stained by fluorescent conjugated antibodies against mouse **Ly6G** (PE), **CXCR2** (FITC) and its isotype control IgG2a,κ (FITC). Un-paired student's t-test was conducted (E), and statistical significance was considered at a level of *P*-value < 0.05.

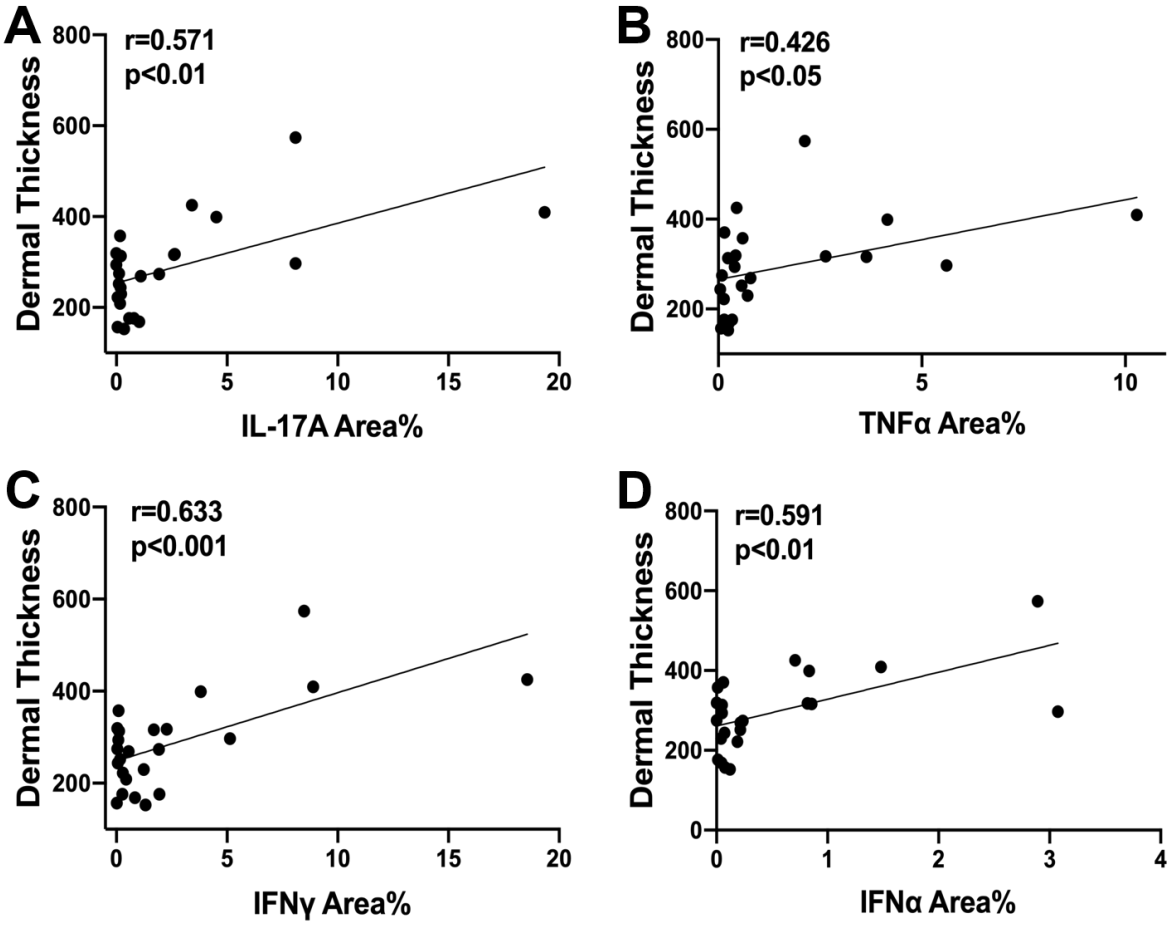

Supplemental Fig 3. A-D. Correlation between NET-associated IL-17A (Area %), TNFα, IFNγ, or IFNα and dermal thickness in all groups of BMT experimental mice. Pearson correlation analysis was conducted to analyze correlation between NET-associated cytokines and dermal skin thickness.

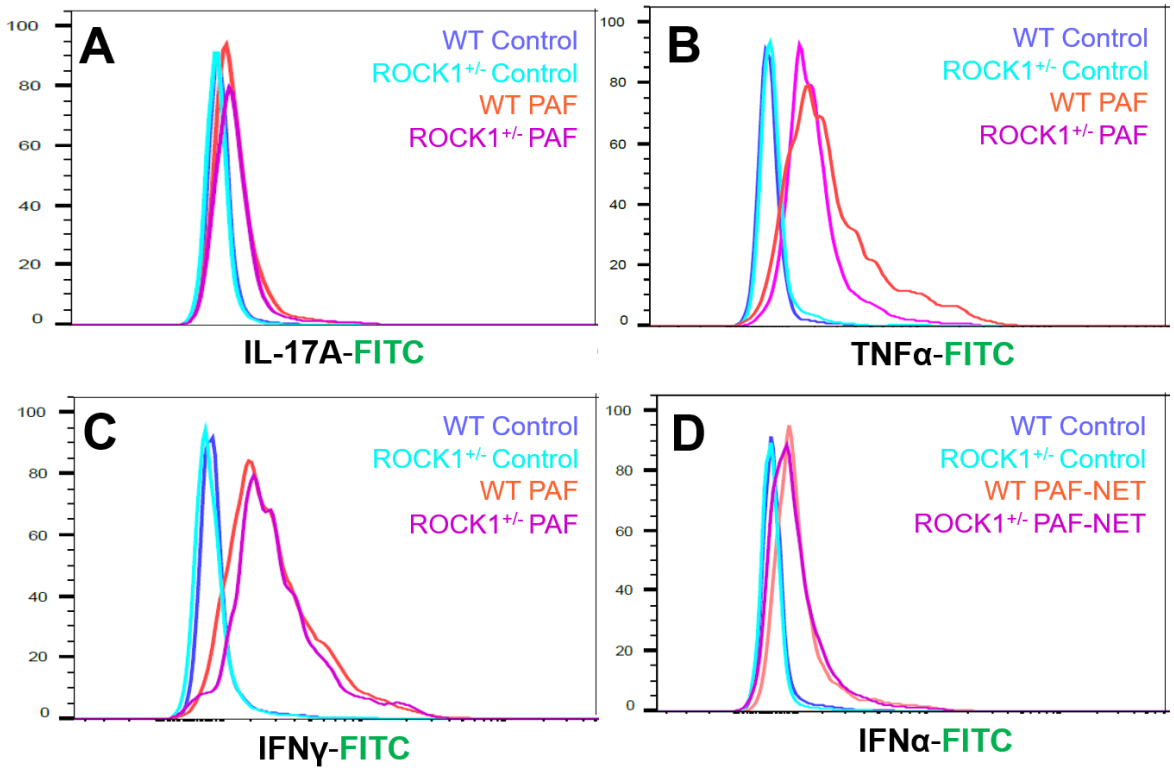

Supplemental Fig 4. A-D. Representative histograms of flow cytometry analyses of BM neutrophils, from ROCK1$^{+/-}$ mice or their WT littermates, which were treated without or with 10 μM PAF (for IFNα induction in panel **D**, treatment with PAF and NETs isolated from cultured neutrophils of MRL/lpr mice) for 20h, then fixation and staining with PE-conjugated anti-mouse **Ly6G**, and FITC labeled anti-mouse **IL-17A**, **TNFα**, **IFNγ**, or **IFNα,** following by flow cytometry analyses (Summary data, see Fig 6A,D,G,J).